NUCLEAR SPIN MEDIATED LANDAU-ZENER TRANSITIONS IN DOUBLE QUANTUM DOTS

CHRISTIAN DICKEL

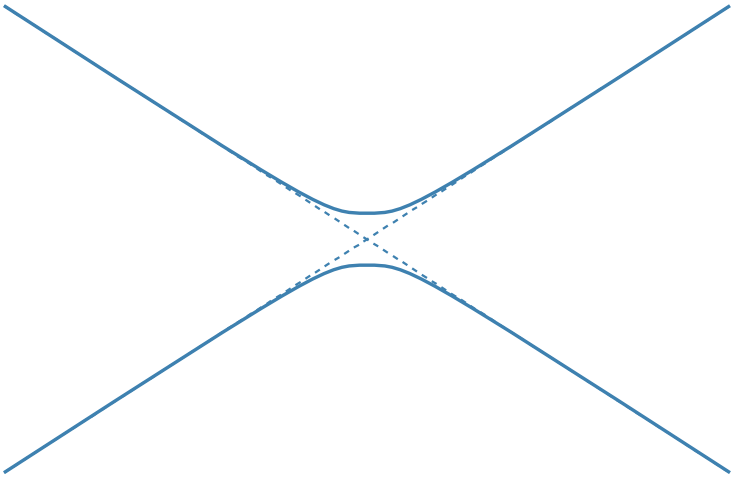

Master's Thesis in Physics
presented to
RWTH Aachen University
The Faculty of Mathematics, Computer Science and Natural Sciences
Department of Physics, Institute II C

September 2013

supervised by
Hendrik Bluhm

To Twickers, the cat who lives.

ABSTRACT

The Double Quantum Dot system in Gallium Arsenide is a promising hardware for quantum information processing. In this thesis, I will present a measurement scheme to probe the dynamics of nuclear spins in Gallium Arsenide quantum dots. The nuclear spins in this system are used for qubit control, but they are also an important source of noise. Subsequently, it is shown that nuclear spin dynamics can be probed by measuring the temporal correlations of single Landau-Zener sweeps across the S-T_+ transition. A semi-classical model of the nuclear spins is sufficient to understand these dynamics. The dynamics are due to the relative Lamor precession of the nuclear spin species in GaAs in the external magnetic field. In the presence of spin orbit coupling, oscillations with the absolute Lamor frequencies are expected. Observations of the latter could be useful to quantify spin orbit coupling.

ACKNOWLEDGMENTS

First I would like to thank Hendrik Bluhm for taking me into his group and giving me this project. The project combines fascinating theoretical physics with a system where the theory can be put to the test. I am sad to leave without trying out the measurent scheme presented here myself. Hendriks clear views of Quantum Information have helped me to feel at home in this diverse and exciting community.

But the year in the Bluhm group was great because of the people that make up this group. I would like to thank Jennifer Arps, Tim Botzem, Jan Bußmann, Pascal Cerfontaine, Thomas Fink, Farshad Foroughi, Mohammed Hamouda, Barbara Hohenbichler, Tim Leonhardt, Marian Marx, Robert McNeil, and Lars Schreiber for the pleasant working atmosphere, fascinating discussions about scientific and non-scientific subjects and advice and help whenever I needed it.

Also I would like to thank Sebastian Mehl, David DiVincenzo and Fabian Hassler from the theory department for helpful discussions.

I would like to thank Pascal Kaienburg for proofreading this thesis.

My parents have payed my way through college and have always given me their support when I needed them. Even more importantly, I know that my family loves me no matter what.

Last but not least, I would like to thank Jasmin. During the stressful time that ends with this thesis, I have not been the best boyfriend of all worlds, but she has kindly overlooked that. I will not remember this year as the year of my master thesis, but as our first year together.

CONTENTS

1 MOTIVATION AND OVERVIEW 1

2 INTRODUCTION TO QUANTUM INFORMATION 3
- 2.1 The Qubit 3
- 2.2 Multiple Qubits 5
- 2.3 Noise and Decoherence 6
  - 2.3.1 Relaxation 7
  - 2.3.2 Dephasing 7
  - 2.3.3 Leakage 7
  - 2.3.4 Quantum Error Correction 8
- 2.4 The DiVincenzo Criteria 8
- 2.5 Quantum Dots as Qubits 8

3 DOUBLE QUANTUM DOT QUBITS 11
- 3.1 Lateral Quantum Dots in Gallium Arsenide 12
- 3.2 Double Quantum Dot Hamiltonian 13
  - 3.2.1 Spin Orbit Interaction 14
  - 3.2.2 Model for the nuclear spins 15
  - 3.2.3 The two electron subspace 17
- 3.3 $S - T_0$ Qubit 19
  - 3.3.1 Initialization and Readout 19
  - 3.3.2 Dynamic Nuclear Polarization 20
  - 3.3.3 Manipulation 21
  - 3.3.4 Relaxation 22
  - 3.3.5 Two Qubit Gates 22
  - 3.3.6 Summary 23

4 LANDAU-ZENER PHYSICS AT THE S-T_+ TRANSITION 25
- 4.1 The Landau-Zener Formula 25
  - 4.1.1 The $S - T_+$ Transition 26
  - 4.1.2 Nuclear Spin Averaged Landau-Zener Probability 27
  - 4.1.3 Finite Sweep Effects 29
  - 4.1.4 Diagonal Noise - Electrical Noise 30
- 4.2 Correlation of Landau-Zener Sweeps 32
  - 4.2.1 $\boldsymbol{T}$-matrix method 33
- 4.3 Experimental results 37
- 4.4 Investigating the spin orbit interaction 39
- 4.5 Stückelberg Interferometry 39
- 4.6 Remarks on the S-T_+ Qubit 42

5 CONCLUSION AND OUTLOOK 45

BIBLIOGRAPHY 47

1 MOTIVATION AND OVERVIEW

In this thesis, I will present a measurement scheme to probe the dynamics of nuclear spins in Gallium Arsenide quantum dots. These dynamics also allow separating nuclear spin and spin-orbit effects, which is otherwise complicated, because both effects act as effective magnetic fields. The physical system studied here is not something found in nature, but it is a device deliberately fabricated to have certain properties. Every part of the physical system is studied with the goal of constructing a controllable two level quantum system, a qubit, with the long term goal of building a quantum computer out of these qubits. Therefore, I will give a brief introduction to quantum information in chapter 2. Then I will introduce the specific system studied here in chapter 3. In chapter 4.1, I will explain Landau Zener physics, a necessary premise for the measurement scheme and finally explain the scheme and present proof of principle experimental results.

FUNDAMENTAL PHYSICS WITH A VISION

> Most probably our increasing ability to juggle with atoms, molecules, photons (and mesoscopic artificial atoms) will lead to applications... Even more probably, these applications will not be the ones we dream about today... [1]
>
> — Serge Haroche

During my year as an exchange student in Brussels in 2010, it so happened that Serge Haroche gave a series of lectures on cavity QED where I first encountered the concept of Quantum Information. Now, in the year of my master's thesis, Haroche shared the 2012 Nobel Prize in Physics with David Wineland for their "ground-breaking experimental methods that enable measuring and manipulation of individual quantum systems". Haroche has been skeptical of a quantum computer at first [1] and it is only fitting that he was the first to quantitatively measure the decoherence of a quantum superposition [2], which is the main reason for skepticism. Still, his lectures inspired me to focus on quantum information, which was greatly facilitated by David DiVincenzo and Hendrik Bluhm joining the RWTH Aachen University staff in 2011. I was drawn to the subject for two different

1 Inaugural Solvay Lecture, Brussels 2010

reasons: The fundamental physics of controlling quantum systems and the vision of quantum information processing.

I was warned from the start, that I should not get my hopes up for a quantum computer. But the field of quantum information would not be the same without the vision of applications. I think of the vision of the quantum computer as an interface, where engineers, computer scientists and physicists meet. We compete in a race to reach milestones on the way to a quantum computer. Still, it is important not to overlook what has already been achieved. Advances in technology have taken us from the conception of quantum mechanics to controllable quantum systems. The strife for more complex controllable quantum systems will give rise to new technologies. Many exciting fundamental problems have been discovered and solved. This is a unique superposition of pure and applied science. It is a privilege that we can perform the thought experiments of the 1920s in the lab today.

2 INTRODUCTION TO QUANTUM INFORMATION

2.1 THE QUBIT

To understand the difference between classical and quantum information, one has to understand the qubit. The word qubit was apparently first used in jest, because it sounds like cubit, an antique unit of length, but by now people are serious when they talk about qubits. The qubit is the basic unit of quantum information in the same way that bits are the basic units of classical information. A qubit is a quantum mechanical two-level system with two basis states, generally called $|0\rangle$ and $|1\rangle$. In contrast to a classical bit that can only take two values, for a qubit any complex linear combination of the two states is a valid state.

$$|\psi\rangle = \alpha\,|0\rangle + \beta\,|1\rangle \;\text{ with }\; |\alpha|^2 + |\beta|^2 = 1$$

The normalization condition ensures that the probabilities of measurement outcomes, that are related to the absolute values of the coefficients, add up to one.

Measurements on a qubit are mathematically written in the form $\langle\psi|\,\widehat{A}\,|\psi\rangle$, $\widehat{A}$ being a hermitian operator that can be expressed as a real linear combination of the Pauli Matrices $\boldsymbol{X}$, $\boldsymbol{Y}$ and $\boldsymbol{Z}$:

$$\boldsymbol{X} = \begin{pmatrix} 0 & 1 \\ 1 & 0 \end{pmatrix},\ \boldsymbol{Y} = \begin{pmatrix} 0 & -i \\ i & 0 \end{pmatrix},\ \boldsymbol{Z} = \begin{pmatrix} 1 & 0 \\ 0 & -1 \end{pmatrix} \tag{2.1}$$

With this condition, a general pure state[1] of the qubit can be written in the form

$$|\psi\rangle = \cos(\theta/2)\,|0\rangle + e^{i\phi}\sin(\theta/2)\,|1\rangle\,,$$

which leads to the visual Bloch sphere representation, seen in figure 2.1. The two angles are the angles of spherical coordinates on the sphere. In the quantum information community the Bloch Sphere plays a unifying role, because all qubits can be represented this way, no matter how they are practically realized. The most well known two-level system is the spin-1/2 particle and other systems are frequently mapped on the spin-1/2 for better intuition. A spin-1/2 couples to magnetic fields. The general Hamiltonian for a spin-1/2 is given by

1 As opposed to mixed states, pure states do not include additional classical uncertainty.

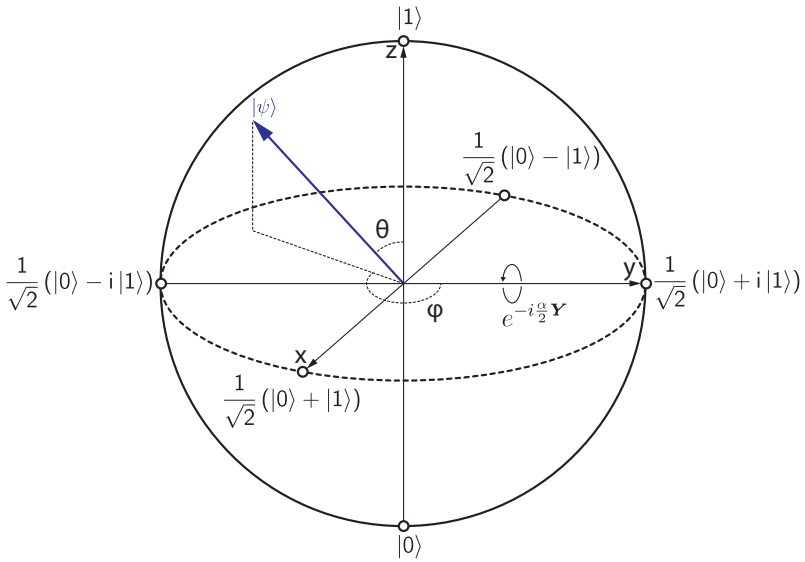

Figure 2.1: The Bloch sphere representation of a qubit. Pure states are vectors on the sphere's surface. Measurements are projections of these states on the respective axis. Rotations around the axis are generated by the Pauli Matrices.

$$\widehat{H} = B_x \boldsymbol{X} + B_y \boldsymbol{Y} + B_z \boldsymbol{Z}.$$

The time evolution in quantum mechanics is given by the Schrödinger Equation

$$i\hbar \frac{\partial}{\partial t} |\psi\rangle = \widehat{H} |\psi\rangle .$$

This can be integrated to yield

$$|\psi(t)\rangle = \underbrace{\mathcal{T} \exp\left(-i \int_{t'=0}^{t'=t_g} \widehat{H}(t')\, dt'\right)}_{U(H(t))} |\psi(0)\rangle$$

with a unitary matrix U, which is a rotation on the Bloch sphere, parametrized by an axis $n = \begin{pmatrix} n_x & n_y & n_z \end{pmatrix}$ and an angle θ. $\mathcal{T}$ is the time ordering operator which makes it easier to write this down in a closed form. In case of a constant magnetic field, the spin precesses around that field with an angular frequency $\omega = g\mu_B |B|$ given by the strength of the magnetic field. Time dependent magnetic fields can be used to generate any desired rotation, for example a bit-flip, which is a rotation by π around the x-axis.

Universal single qubit control consists of reliably realizing arbitrary rotations on the Bloch sphere. This does not require arbitrary rotation axes, in fact two distinct axes can be used to generate arbitrary rotations. A spin-1/2 can be controlled with a constant magnetic field B_z in z-direction and a tunable field in the x-direction $B_x(t)$. It is even

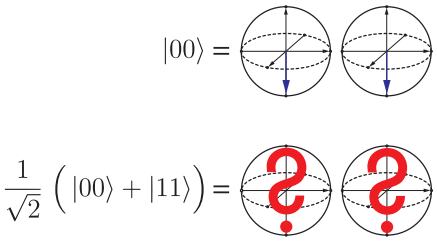

Figure 2.2: More Qubit Representation?

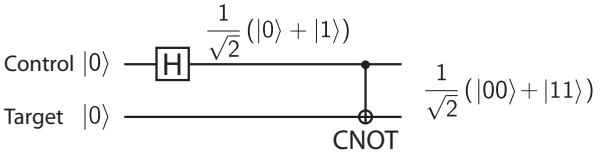

Figure 2.3: Circuit Diagram of the CNOT Gate.

possible to approximate any rotation to arbitrary accuracy by concatenating fixed rotations from a finite set. This was proven by Solovay and Kitaev, a pedagogical introduction to this can be found in [3]. Which of these approaches to quantum control will be optimal depends on the details of a given qubit system.

Not only the manipulation of a qubit is important, any experimental qubit must be initialized and read out. The readout fidelity is ultimately important for the overall qubit fidelity. It is practical to have different readout axes, but usually there is only one. This means that gates need to be performed to map the other axes on the measurement axis and read out. Initialization can in principle be done via projective readout, but alternate faster ways to initialize the qubit with high accuracy are desirable.

2.2 MULTIPLE QUBITS

The Bloch sphere is a useful visualization for one qubit, but there is no generalization for more qubits and this goes to the heart of the complexity of quantum mechanics. A two qubit system cannot be represented by two Bloch spheres. For product states such as $|00\rangle$, it works, but there is no way to display entangled states such as $|00\rangle+|11\rangle$, because the Hilbert space of a two qubit system is four dimensional. There are four complex parameters, thus eight real ones, and the normalization condition and the irrelevance of a global phase only reduce that number to six real parameters. Accordingly, a two qubit system could be represented by three Bloch spheres, but this representation would not necessarily be intuitive.

The additional parameters contain entanglement of the two qubits. An entangled state has perfect correlations between the measurement outcomes of the two qubit, independent of the basis the qubits are measured in. This has no classical analogon. As the complexity scales exponentially with the number of qubits, classical computers fail to simulate large quantum systems.

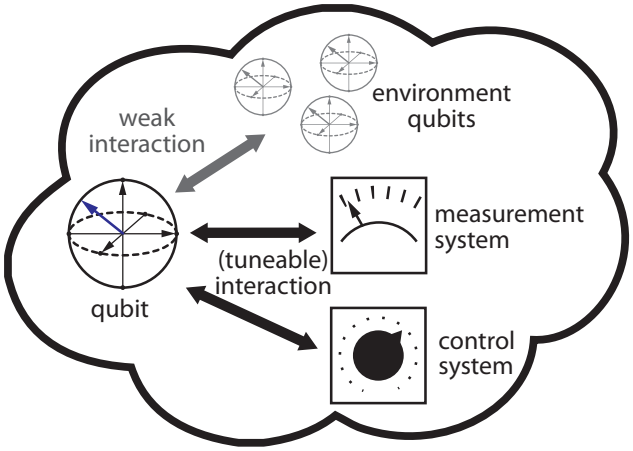

Figure 2.4: Generic Qubit System.

The quantum gates operating on a complete qubit register can be reduced to two qubit gates and one qubit gates, similar to the way gates are decomposed for classical computers. It was shown that arbitrary gates on a quantum register can be efficiently composed from arbitrary single qubit gates and the controlled NOT (CNOT) two qubit gate. A circuit diagram for this gate is found in figure 2.3. This two qubit gate flips the target qubit if and only if the control qubit is in the $|1\rangle$ state. In figure 2.3, the qubits start out in the $|00\rangle$ state, the control qubit is put into an equal superposition by a Hadamard Gate and then the CNOT is applied. The final state is an entangled state, that cannot be factored into a product of states of each qubit. At present, single qubit control has been achieved in many qubit prototype systems, while high fidelity two qubit gates for several qubits remain as a challenge. However, this thesis is only about single qubit physics.

2.3 NOISE AND DECOHERENCE

The transition from fragile quantum information to classical information is a fascinating subject in itself. The CNOT from the previous chapter is a good way to illustrate this. Any environment of a qubit can be modeled by a large number of qubits. The interaction can for example be a CNOT. Thus, the qubit will be entangled with environment qubits. But those qubits may not be measurable for the experimenter. The entangled state after the CNOT in figure 2.3 is a well defined state on the two-qubit system, but looking only at one of the qubits it appears to be a completely mixed state - in any basis, an experimenter measures both basis states with equal probability. Now it is more complicated, because there are a lot of environment qubits with different, even time dependent interactions. In addition the environment qubits interact with each other. Classical behavior emerges

from quantum theory in the limit of many particles and high temperatures - this is related to size and temperature of the environment.

The results of measurements are classical, because the measurement apparatus is a classical system. Individual quantum systems that make up the measurement apparatus cannot be read out, only a collective classical state. During a measurement, apparatus and qubit interact until they are entangled, but this entanglement decays due to the classical nature of the measurement apparatus. The outcome will be a definite state of the qubit and the corresponding signal as a measurement outcome. This is a projective measurement.

2.3.1 *Relaxation*

Over time, the qubit will end up in thermal equilibrium with the environment. It can exchange energy with the environment, changing the polar angle θ in the Bloch sphere representation. Any uncontrolled change in energy will cause the loss of quantum information. This can be measured by preparing the qubit in the excited state and measuring the time it takes to go to thermal equilibrium. The decay constant is generally called T_1.

2.3.2 *Dephasing*

Information in the azimuthal angle ϕ on the Bloch sphere can also be lost to the environment, without energy dissipation. This is called dephasing. There is no classical equivalent for this. The loss of phase can be measured by so called Ramsey Interferometry. The qubit is initialized in the $|0\rangle$ state and brought to the equator of the Bloch sphere by a $\pi/2$ pulse. After a time delay, a second $\pi/2$ pulse along the same axis is applied and the qubit is measured along the z-Axis. During the delay time, the qubit undergoes Lamor precession in the energy subspace. The oscillations decay because of noise. The decay constant of these oscillations is called T_2^*.

If the noise causing this dephasing is slow compared to qubit evolution time, more elaborate sequences of pulses can be used to extend the lifetime of the phase information. This goes by the name of spin-echo sequences and was developed in the context of nuclear magnetic resonance physics. Hence, the dephasing time dependends on the pulse sequence. The upper limit is called T_2.

2.3.3 *Leakage*

If the qubit is encoded in a larger Hilbert space, there can be leakage out of the qubit space. Leakage can be correctable, if the two logical

states leak into two different states, but if the original state cannot be reconstructed, the leakage results in a loss of quantum information.

2.3.4 *Quantum Error Correction*

Contrary to bit errors in classical computing, quantum errors can be arbitrarily small differences in the angles on single qubits or in the relative phases, that would still at a certain point affect the entire register. Intuitively one would assume, that a larger quantum computer is impossible, yet it was shown that a quantum computer can be realized in the presence of initialization, manipulation and readout errors, by introducing redundancy. The additional Qubits and number of operations needed scale polynomially. Any quantum error correction theme has a threshold value for the noise it can correct. During the correction of one qubit, the others should remain coherent, which leads to an estimated threshold of $\sim 10^5$ operations within the coherence time.

2.4 THE DIVINCENZO CRITERIA

The requirements for a physical system to be a good hardware for a quantum computer were summarized by David DiVincenzo [4] to be:

- scalability
- initialization
- universal set of gates
- readout
- coherence time much longer than gate operations
- fidelities above the Quantum Error Correction Threshold

For quantum communication it is additionally useful to have a quantum computing hardware that can couple to optical photons, which can be reliably transmitted over large distances.

2.5 QUANTUM DOTS AS QUBITS

In 1997 Daniel Loss and David DiVincenzo proposed gate defined semiconductor quantum dots as quantum computers [5]. Quantum dots are slots for particles - mostly electrons - that are confined in all three directions, so that there are only discrete energy levels. This is why they are sometimes compared to atoms.

The Loss-DiVincenzo proposal is to use the electron spins of electrons in coupled quantum dots as qubits. They give some first ideas

as to how they could be manipulated and read out. The primary argument for such dots is, that they are very small and based on semiconductor technology that is well developed as the hardware for classical computers.

Using the spin state of a single electron as a qubit is elegant insofar, as it is truly a two level system. In the next years, many of the requirements for the Loss-DiVincenzo proposal were met. Initially GaAs heterostructures were the preferred hardware for electrically manipulated quantum dots, but by now there is progress for dots in silicon and silicon-germanium heterostructures. But in addition to the single-electron-spin qubit, the double quantum dot singlet-triplet qubit and the exchange qubit in triple quantum dots have been introduced. The triple quantum dot qubit could in principle work without an external magnetic field [6, 7], while the double quantum dot qubit that I will describe in detail in chapter 3 can be manipulated solely by using voltage pulses.

3

DOUBLE QUANTUM DOT QUBITS

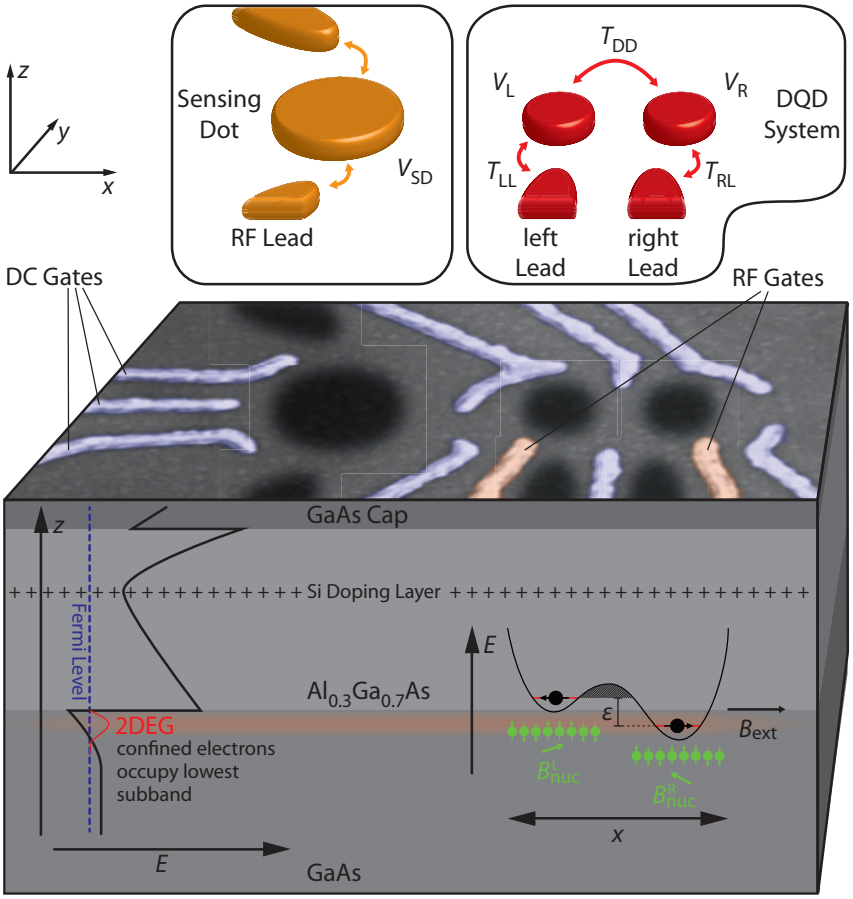

Figure 3.1: Visual Overview of the Double Quantum Dot System: This figure contains four figures in one - illustrating the complexity of the system. A (modified) scanning electron microscope picture of the electric gates ties the picture together. RF gates are colored in orange and DC gates in blue. Below this, a scheme of the heterostructure with the conduction band edge as a function of depth z, electrons in the triangular potential well at the interface form the 2DEG. On the lower right a cut through the electrostatic potential in x-direction is displayed. Above, there is an abstract depiction of the dots and leads for the DQD system and the sensing dot. Each of these parts will be explained in the following.

Why is the title of this section in plural? The level diagram of a double quantum dot containing two electrons is big enough for different qubit encodings, but this will be explained at the end of the section.

I will first briefly explain the physical realization of lateral Quantum Dots in a GaAs-AlGaAs heterostructure. In this context, I will also explain charge sensing with a sensing dot, that is necessary for the readout of these dots. Then, I will explain the theoretical Hamiltonian of the Double Quantum Dot (DQD) System along with hyperfine and spin-orbit interaction. Gate design and tuning form the bridge between a concrete device and the abstract target Hamiltonian. In the end, the S-T_0 qubit will be explained.

3.1 LATERAL QUANTUM DOTS IN GALLIUM ARSENIDE

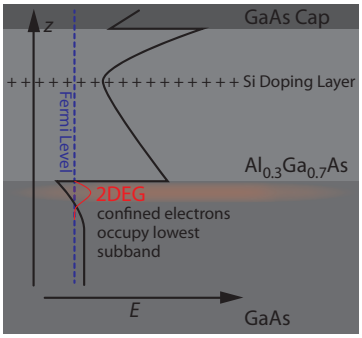

Figure 3.2: GaAs-AlGaAs heterostructure

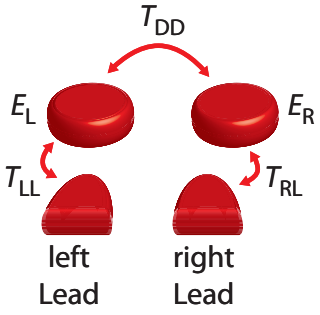

Figure 3.3: DQD Parameter Scheme

There are different ways to realize the three dimensional confinement of electrons. In semiconductors, there are self assembled dots due to island growth, that are usually manipulated optically and gate defined dots in heterostructures, which are the subject of this thesis. Additionally there are gate defined and etched graphene quantum dots and gate defined quantum dots in nanowires.

In this thesis I will focus on gate defined quantum dots. Gate defined quantum dots begin with a two dimensional electron gas (2DEG) that provides confinement in one dimension. GaAs and AlGaAs have very similar lattice constants and can be epitaxially grown with atomically smooth interfaces. But AlGaAs has a larger band gap. A Silicon doping layer or a metallic top gate curve the conduction band edge so that it drops below the Fermi level at the AlGaAs-GaAs interface. At the interface, electrons from the dopands or the top gate accumulate. The triagonal potential well at this point needs to be sufficiently small, so that only the lowest energy sub band is occupied. This forms the 2DEG.

Above a GaAs cap layer, electrical gates are written with electron beam lithography. These gates are used to confine the electrons in the other two dimensions in a controllable manner. The 2DEG split in different regions by these gates, so that certain parts of the 2DEG can be contacted to form controllable leads to the quantum dots. The shadows in figure 3.1 indicate the regions where the 2DEG is not depleted.

The DQD System consists of two quantum dots, each coupled to a lead. Only the DC Gates are used for tuning. There are six DC gates, that are supposed to tune five parameters visualized in figure 3.3: The two energies of the dot ground states, the two tunnel couplings to the leads and the tunnel coupling between the dots. In addition a positive bias can be applied to the entire 2DEG, which can be seen as

an additional gate. The RF gates are used for fast manipulation of the ground state energies of each dot. They are kept apart from the DC gates, because applying a bias voltage and sending microwave pulses through the same gate can be problematic. Changing the detuning with these gates has proven to be a reliable control method for the DQD system.

The charge states of the DQD can be read out with a nearby charge sensor. In the gate design in figure 3.1, gates for a sensing dot are fabricated close to the DQD, which will be explained in section 3.3.1.

So the DQD is the qubit in the generic scheme from last chapter, the control system is the RF gates and the sensing dot is the measurement system. The environment is made up of the nuclear spins, phonons and photons in the coaxial cable leading to the RF gate. The charge configuration in the doping layer couples to the DQD and jumps in this transition might require a retuning of the dots.

3.2 DOUBLE QUANTUM DOT HAMILTONIAN

The methods described in section 3.1 can be sufficiently perfected to create two tunable slots for electrons sufficiently close to each other and operate them in the single electron regime. It is assumed, that the dots could be coupled to leads to introduce electrons into the system, but during dot operations, the coupling to the leads is turned off. Therefore the leads are neglected in the following. The electronic Hamiltonian can be constructed of several parts, as in the appendix of [8] and in [9]:

$$H^e = H_{SP} + H_C + H_T + H_Z^e + H_{HF}^e + H_{SO}$$

In second quantization these parts can be written down intuitively. In my notation the index $l \in \{L, R\}$ denotes the orbital state, the orbitals are Wannier Orbitals for the left and right dot. The index $\sigma \in \{\uparrow, \downarrow\}$ designates the spin component with respect to the external magnetic field. The creation and annihilation operators $a_{l\sigma}^\dagger$ and $a_{l\sigma}$ accordingly create and destroy electrons in dot l with spin σ. The number operator $n_{l\sigma} = a_{l\sigma}^\dagger a_{l\sigma}$ counts the number of electrons in orbital l with spin σ.

- $H_{SP} = \sum_l V_l \, n_{l\sigma}$
  Single particle charging energy, V_l depends on the size of the respective dot.
- $H_C = U \sum_l n_{l\uparrow} n_{l\downarrow} + U' \left(n_{L\uparrow} + n_{L\downarrow}\right) \left(n_{R\uparrow} + n_{R\downarrow}\right)$
  Electron-electron coulomb interaction, U is the inter dot Coulomb interaction, depending on the size of the respective dot, and U'

is the intra dot Coulomb interaction, depending on the spacing between the dots.

- $H_T = T_{DD} \sum_{\sigma} \left(a^{\dagger}_{L\sigma} a_{R\sigma} + a^{\dagger}_{R\sigma} a_{L\sigma} \right)$
  Tunneling between the dots. T_{DD} depends on potential landscape and can be varied by gate voltages.

- $H^e_Z = \frac{1}{2} g \mu_B B_{ext} \sum_{l} \left(n_{l\uparrow} - n_{l\downarrow} \right)$
  Electron Zeeman energy, the negative g-factor of GaAs favors alignment with the magnetic field.

- $H^e_{HF} = \sum_{l} \mathbf{S}_l \cdot \mathbf{h}_l$
  hyperfine coupling to the nuclear spins. $\mathbf{S}_l$ is the spin $\mathbf{h}_l = \sum_{n=1}^{N} A_n \left| \Psi \left(\mathbf{R}_n \right) \right|^2 \mathbf{I}_n$ is the Overhauser Field in the respective dot. This is a Spin non-conserving interaction. I will explain this in more detail in section 3.2.2.

- $H_{SO} = \frac{i}{2} \mathbf{\Omega} \sum_{\sigma_1, \sigma_2 = \uparrow\downarrow} \left(a^{\dagger}_{L\sigma_1} \boldsymbol{\sigma}^{\sigma_1 \sigma_2} a_{R\sigma_2} + a^{\dagger}_{R\sigma_2} \boldsymbol{\sigma}^{\sigma_1 \sigma_2} a_{L\sigma_1} \right)$
  Spin orbit coupling. There are spin flip tunneling processes, so it is a spin non-conserving interaction. $i\mathbf{\Omega} = \langle \Phi_L | p_{\tilde{\xi}} | \Phi_R \rangle \boldsymbol{a}_{\mathbf{\Omega}}$, $\boldsymbol{a}_{\mathbf{\Omega}}$ depends on the orientation of the crystal axes. I will explain this in more detail in section 3.2.1.

I will explain how effective magnetic fields arise from spin-orbit interaction and the nuclear spins in the following subsections. Especially the nuclear spin effective fields display complex behavior, caused by the microscopic effects that lead to these fields. From then on, I will treat the fields semi-classically.

3.2.1 *Spin Orbit Interaction*

A good detailed summary of spin orbit coupling in GaAs quantum dots can be found in [10] and a shorter discussion in the review [11].

The Zeeman split levels of the dots are only weakly influenced by spin orbit coupling, because the confinement is much smaller than the spin flip length. Therefore spin orbit coupling mainly manifests itself as a spin flip tunneling process between the dots. The spin of an electron traveling ballistically in the 2DEG plane rotates depending on the distance traveled. One can define the spin orbit distance as the distance it takes for a full rotation.

But for the estimation of direction and strength of spin orbit coupling, it is important to understand where it comes from. Spin orbit coupling in GaAs Heterostructures springs from two different sources: Firstly, at the interface there is a strong electric field in z-direction through which the electrons move. A particle moving in an

electric field experiences a magnetic field, because electric fields in the rest-frame transform into magnetic fields in a moving frame. This term has the form $\boldsymbol{B} \propto \boldsymbol{p} \times \boldsymbol{E}$ and is called Rashba term in figure3.4. If the 2DEG is induced by a top gate, this term could be tuned. This would lead to a term perpendicular to the dot-dot axis in the 2DEG plane:

$$H_R = \alpha \left(-p_y \boldsymbol{X} + p_x \boldsymbol{Y}\right)$$

Secondly, the electron experiences the electric fields of the atoms of GaAs. The zinc blende structure of GaAs is not symmetric under inversion. For x, y and z corresponding to the crystal directions (100), (010) and (001), this leads to a term of the form

$$H_D = \beta \left(-p_x \boldsymbol{X} + -p_y \boldsymbol{Y}\right)$$

For other growth directions this term would look different. The strength of the Rashba and Dresselhaus contribution depends on the Heterostructure, but the direction of the dot-dot axis with respect to crystal orientation will decide whether they have the same sign. This should be kept in mind in device design. In conclusion, there is a fixed effective magnetic field from spin orbit coupling, that scales with the tunnel coupling and

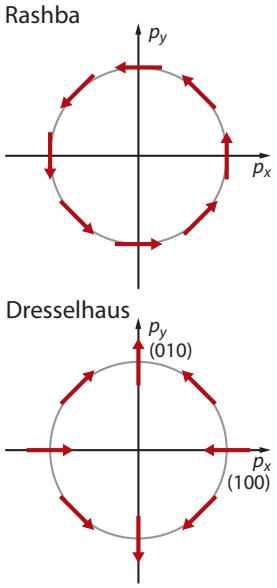

Figure 3.4: effective SO field as a function of momentum

3.2.2 *Model for the nuclear spins*

A review of nuclear spins in semiconductor quantum dots can be found in [12]. The nuclear spin model used here was presented in [13]. The electron interacts with the nuclear spins mainly via Fermi contact interaction, this means, that the interaction with each nuclear spin is scaled by the electron wave function at the nucleus:

$$H_{HF}^{e} = \sum_{n=1}^{N} A_n \left|\Psi\left(\mathbf{R}_n\right)\right|^2 \mathbf{I}_n \cdot \mathbf{S}$$

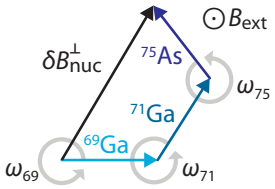

Figure 3.5: nuclear spins perpendicular to external field

Dot parameters suggest that electron wave function covers about two million unit cells, which is supported by experimental evidence [14]. The nuclear Zeeman splitting is less than 1 mK in temperature, so even in a dilution refrigerator temperatures the nuclei are highly disordered. Thus, the effective magnetic field experienced by the electrons results from a random walk with $\sim 10^6$ steps. A semi classical

	Abundance $(^{nuclei}/_{\text{unit cell}})$	A (μeV)	ω $(\mu s^{-1}\, T^{-1})$
Ga_{69}	0.601	36.00	-64.2
Ga_{71}	0.399	46.01	-81.6
As_{75}	1.000	42.98	-45.8

Table 3.1: the nuclear spin species in GaAs

approach is adequate due to the large number of nuclei and the high temperature.

There are three relevant isotopes in GaAs that each contribute to $\boldsymbol{B}_{\text{nuc}}$ as shown in figure 3.5. The nuclear spin parameters taken from [15] can be found in table 3.1. ^{69}Ga, ^{71}Ga and ^{75}As, all nuclear spin $3/2$. In the homogenous coupling approximation, the expected effective field of each species can be approximated as normally distributed in each component with standard deviation $B_i^x = B_i\sqrt{N_i/3}$, where i denotes the species, N_i is the number of nuclei of species i, B_i is the size of each step in the random walk. The step size scales inversely with the total number of nuclei the electron couples to $B_i = {}^5/_2 \cdot \frac{A_i}{N}$, because a more extended wave function will mean less weight near each nucleus. With these assumptions, expectation values of the nuclear spin field can be calculated. For two million unit cells in each dot, the $\left\langle \left(\delta B^{\perp}\right)^2 \right\rangle^{1/2}$ should be on the order of 4 mT. This leads to a loss of coherence for electron spins on the scale of $\sim 10\,\text{ns}$.

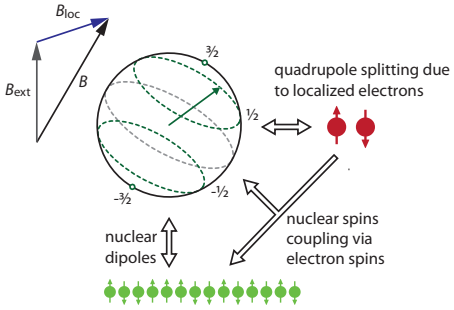

Figure 3.6: local field changing precession axis and frequency of individual nuclei

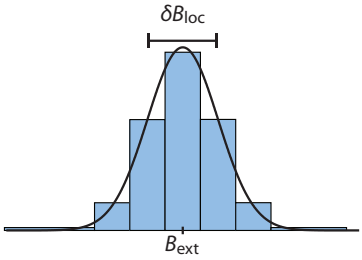

Figure 3.7: magnetic field distribution can be discretized

Now the nuclei are not only in a disordered state, but they also exhibit dynamics in the external fields, as suggested in figure 3.5. It is crucial that they have different precession frequencies, which leads to fluctuations in the magnitude of the nuclear spin field. The oscillations happen on a μs scale, electron dynamics are much faster, this means that for electron time evolution one can usually assume a fixed random variable for the nuclear field.

For dynamics of the effective nuclear spin field, one has to keep in mind, that it is made up of individual nuclei. Each individual nucleus experiences a magnetic field that comes from the external field plus an individual local field. This field comes from the other nuclei, that couple to the individual nucleus via the electrons and via their dipole components. There is an additional quadrupole splitting, that comes from the localized electrons . These local

fields are normal distributed with a standard deviation of $\delta B_{\text{loc}} = 0.3\,\text{mT}$ [16]. Therefore, the nuclear spin dynamics dephase over time. To include this in a nuclear spin model neglecting the change in precession axis, one can introduce artificial nuclear spin subspecies with slightly different frequencies $\omega_i = \gamma_i \left(B_{\text{ext}} + \delta B_{\text{loc},i}\right)$. To do this, one discretizes the normal distribution. The number of spins in the subspecies has to be weighted by the normal distribution. Nuclear dephasing times are on the order of $80\,\mu\text{s}$. The number of additional species should not be chosen arbitrarily small, because a species should contain enough nuclei to justify the semi-classical treatment. It has turned out that introducing more than five additional species does not induce significant changes, therefore I stuck to five subspecies. I have always assumed that the electron wave function covers two million unit cells in accordance with [14].

It is important to note, that I have neglected changes in the wave function. In principle any change in the wave function will change the nuclei the electrons couple to and introduce additional noise into the nuclear spin effective fields. The pulses in detuning only wiggle the dots a little and this effect should not be dominant but it is there and stands in the way of nuclear spin control. Also I have neglected the effect of nuclear spins in the barrier, that the electron could see during a tunnel process. This would add to spin flip tunneling, but be isotropic in the direction of the external field and might thereby be distinguished from spin orbit interaction.

3.2.3 *The two electron subspace*

The second quantization terms above can be used to write down the DQD Hamiltonian for any number of electrons, but in this thesis the focus is on the two electron subspace, although there has been recent work on quantum dots with higher occupation numbers [17, 18] For the two electron subspace, an effective Hamiltonian can be derived from the second quantization terms given above. There are six states, three singlet and three triplet states. The quantization axis is chosen in the direction of the external magnetic field. It is chosen in the 2DEG plane, because a perpendicular field could change the 2DEG properties. But I call this the z-direction now, which is inconsistent with the coordinate system used before. In heterostructures the growth direction is usually the z-direction, and in DQD Qubits standard direction for the magnetic field is the z-direction.

The full Hamiltonian for this system is adapted from [9]:

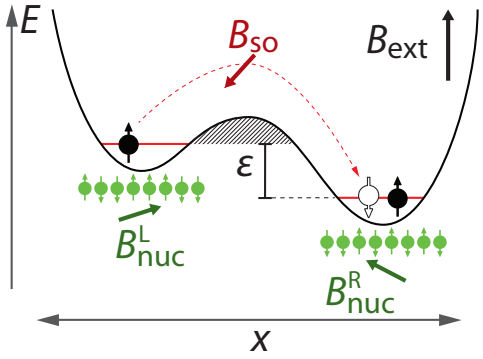

Figure 3.8: Double quantum dot potential and effective magnetic fields

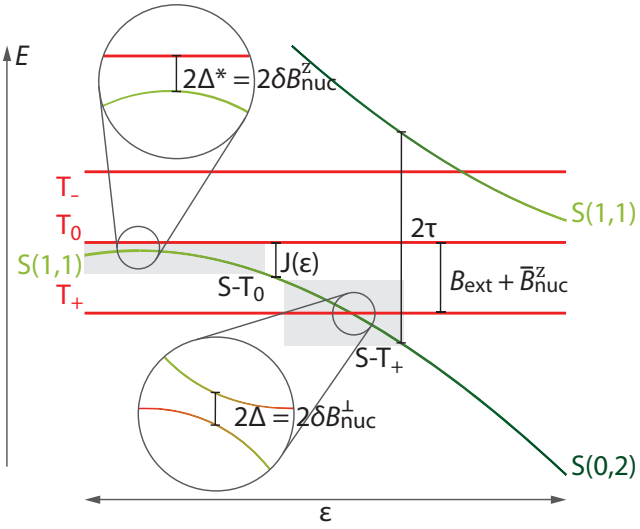

Figure 3.9: Double quantum dot Energy Levels. Transfer function $J(\varepsilon)$ gives difference between $|S(1,1)\rangle$ and $|T_0\rangle$. Grey areas mark the operation space of the S-T_0 and S-T_+ qubit

basis: $[|S(0,2)\rangle, |S(2,0)\rangle, |S(1,1)\rangle, |T_+\rangle, |T_0\rangle, |T_-\rangle]$

$$\boldsymbol{H} = \begin{pmatrix} U-\varepsilon & 0 & -\sqrt{2}\,T_{DD} & -i\sqrt{2}\,\Omega & 0 & -i\sqrt{2}\,\Omega \\ 0 & U+\varepsilon & -\sqrt{2}\,T_{DD} & -i\sqrt{2}\,\Omega & 0 & -i\sqrt{2}\,\Omega \\ -\sqrt{2}\,T_{DD} & -\sqrt{2}\,T_{DD} & V_+ & -\sqrt{2}\,\delta B^+_{nuc} & \delta B^z_{nuc} & \sqrt{2}\,\delta B^-_{nuc} \\ i\sqrt{2}\,\Omega & i\sqrt{2}\,\Omega & -\sqrt{2}\,\delta B^+_{nuc} & V_- + B_{ext} + \bar{B}^z_{nuc} & \sqrt{2}\,\bar{B}^-_{nuc} & 0 \\ 0 & 0 & \delta B^z_{nuc} & -\sqrt{2}\,\bar{B}^+_{nuc} & V_- & \sqrt{2}\,\bar{B}^-_{nuc} \\ i\sqrt{2}\,\Omega & i\sqrt{2}\,\Omega & \sqrt{2}\,\delta B^-_{nuc} & 0 & -\sqrt{2}\,\bar{B}^+_{nuc} & V_- - B_{ext} + \bar{B}^z_{nuc} \end{pmatrix}$$

Parameters are the single particle level difference ε, the intra dot coulomb interaction U, the singlet and triplet inter dot coulomb interactions V_+ and V_- (they are slightly different because the wave functions are slightly different). The singlet subspace is strongly coupled by the tunnel coupling and the hybridized singlet levels depend strongly on the detuning. The triplet subspace is split by fields in the z-direction. The triplet has a symmetric spin state, the wave function needs to be antisymmetric. Accordingly the triplet states are all in the (1,1) charge configuration and the ε has no effect on triplet energies.

The red matrix elements are spin non-conserving. Spin orbit interaction couples the $m = \pm 1$ triplet states with the $|S(0,2)\rangle$ and $|S(2,0)\rangle$ singlet state. The triplet subspace is coupled by the mean perpendicular field of both dots, $\bar{B}^{\pm}_{nuc} = 1/2\left(\bar{B}^x_{nuc} \pm i\bar{B}^y_{nuc}\right)$ with $\bar{B}^x_{nuc} = 1/2\left(B^{R,x}_{nuc} + B^{L,x}_{nuc}\right)$. The $m = 0$ triplet state is coupled to the $|S(1,1)\rangle$

state by difference fields between the dots $\delta B^{+}_{nuc} = 1/2\left(\delta B^{x}_{nuc} \pm i\delta B^{y}_{nuc}\right)$ with $\delta B^{x}_{nuc} = 1/2\left(\delta B^{R,x}_{nuc} - \delta B^{R,y}_{nuc}\right)$.

The level diagram can be found in figure 3.9. The energy difference between the hybridized ground state singlet $|S^*\rangle$ and $|T_0\rangle$ can be approximated by an exponential function [19]:

$$J = E_{S^*} - E_{T_0} = J_0 \exp\left(-\frac{\varepsilon}{\varepsilon_0}\right) \tag{3.1}$$

This function is called transfer function in the following. The exponential model is merely phenomenological, but holds well close to $|T_0\rangle$.

3.3 S − T$_0$ QUBIT

There are different ways to encode a qubit in this Hamiltonian described in section 3.2.3. Experimentally it has turned out, that the single dot level energies can be dynamically manipulated with the AC gates in figure 3.1. The tunnel coupling is more fragile and is kept fixed. The external magnetic field can only be changed slowly, so it is also kept fixed.

3.3.1 *Initialization and Readout*

A singlet can be initialized fast by tuning the dot to large detuning and turning on tunneling from a lead. If the detuning is such that only the lowest state in the dot may be occupied, two electrons will tunnel in and form a singlet state.

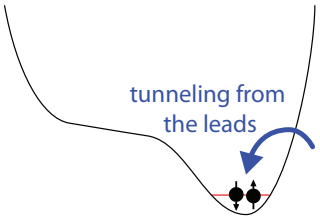

Figure 3.10: Initialization

Readout of the state is based on spin to charge conversion. The singlet ground state will be in the (1,1) or (0,2) state depending on detuning, while the triplet state remains in the (1,1) state until additional electron levels become relevant. The charge state of the DQD can be read out with a nearby quantum dot. This sensing dot, operated in the few electron Coulomb blockade regime, is used as a charge sensor. Coulomb blockade means that there is no transport because the capacitive energy of an additional electron is higher than the bias voltage. The sensing dot levels depend on the charge environment, especially of course on the DQD. If tuned in the right way, transport through the sensing dot can be used to read out the DQD charge state. This can be combined with high frequency equipment for a fast reliable single shot readout of the charge state.

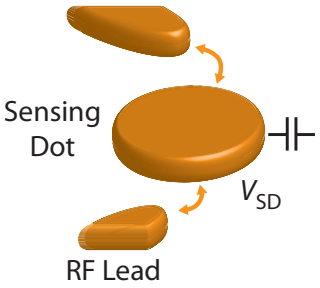

Figure 3.11: Sensing Dot. The capacitor indicates capacitive coupling to DQD

A quantum point contact (QPC) is a more primitive charge sensor, essentially just a narrow tunnel barrier between two

2DEG regions that displays quantization in conductivity. The tunnel barrier depends on the DQD state. QPCs are less sensitive than sensing dots and require longer averaging times. The measurements presented in this thesis were measured with a QPC, but future measurements will be taken with a sensing dot.

3.3.2 *Dynamic Nuclear Polarization*

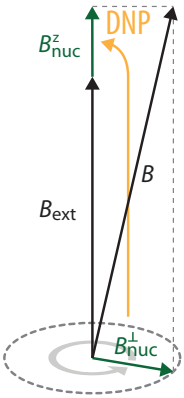

Figure 3.12: DNP Schematic

Nuclear spin control plays an important role in both gate defined and self assembled quantum dots [20, 21, 22]. In gate defined dots, the electronic system can be rapidly initialized in a singlet state and the current state can be easily discarded by emptying the dots. This allows manipulating the nuclear spins into a non-equilibrium state via the electronic system. The electron hyperfine interaction can be rewritten in terms of highering and lowering operators:

$$\boldsymbol{S}\cdot\boldsymbol{I} = {}^1\!/_2\underbrace{\left(I^+S^- + I^-S^+\right)}_{\text{flip flops}} + I^zS^z$$

Whenever the electron goes from a $m = 0$ to an $m = \pm 1$ state, the angular momentum has to be conserved. If the spin flip is caused by hyperfine interaction, a nuclear spin flops to guarantee the conservation of angular momentum. This phenomenon is called dynamic nuclear polarization (DNP).

Dynamic nuclear polarization was first measured in spin blockade transport experiments [23], but soon specific pulse sequences were used to pump the nuclear spin state.

The perpendicular component of the local fields will reduce any build up nuclear polarization over time. Thus DNP schemes need to polarize faster then this depolarization mechanism works. At first this was done through adiabatic passage through the S-$T^{\pm}$ transition[24]. There are also methods using non-adiabatic Landau-Zener pulses as explained later in this thesis. Also there have been approaches using continuous wave driving to control the nuclear spins [25].

It has been found that not only the mean nuclear spin field along the external field direction can be pumped, but also the difference field $\delta B^z_{\text{nuc}} = \delta B^R_{\text{nuc}} - \delta B^L_{\text{nuc}}$ [26]. This happens, because the nuclear spin flops occur mostly in one of the dots, likely because of different dot size and thus different coupling to the nuclei. This is instrumental for S-T_0 qubit control.

It is possible to measure the mean or gradient Overhauser field using the electrons as a probe and then pump depending on the mea-

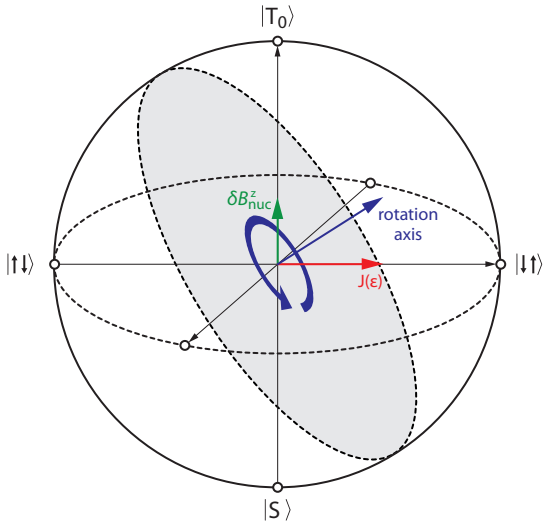

Figure 3.13: S-To Qubit Bloch sphere. The $J(\varepsilon)$ can be changed, the ΔB^z_{nuc} can be set to a fixed value with DNP. Pulse sequences in ε allow arbitrary rotations on a ns timescale.

surement outcome. This feedback DNP has allowed to set the Overhauser fields to desired values and suppress fluctuations[16].

However, there are still open questions on DNP. The performance of such DNP schemes is currently limited by a low spin transfer probability from electrons to nuclei [16], which is presently not understood. It was observed that the electron spin flip rate exceeds the nuclear polarization rate, which may result from an additional SO spin flip channel [27, 28, 29]. Probing the transitions between S and T_+ states and the role of SO coupling is thus also relevant for understanding the limitations of DNP methods.

3.3.3 *Manipulation*

Now there are singlet initialization and singlet triplet readout. Along with nuclear spin control one can use this to achieve a functional qubit. One can chose the $|S\rangle$ and $|T_0\rangle$ states as logical states:

$$\begin{aligned} |S\rangle &= \frac{1}{\sqrt{2}}\left(|\uparrow\downarrow\rangle + |\downarrow\uparrow\rangle\right) \\ |T_0\rangle &= \frac{1}{\sqrt{2}}\left(|\uparrow\downarrow\rangle - |\downarrow\uparrow\rangle\right) \end{aligned}$$

As explained in section 3.3.2, the nuclear spins can be controlled, so one can set the δB^z_{nuc} to a certain value. At $\varepsilon = 0$, $|T_0\rangle$ and $|S\rangle$ are nearly degenerate. They are coupled by δB^z_{nuc} which drives rotations between the $|\uparrow\downarrow\rangle$ and $|\downarrow\uparrow\rangle$ states. If one changes ε in either direction one increases the energy difference between $|S\rangle$ and $|T_0\rangle$, because

the singlet state energy is lowered. The Hamiltonian on the qubit subspace reads:

$$H = \frac{\delta B^z_{\text{nuc}}}{2}\boldsymbol{Z} + \frac{J(\varepsilon)}{2}\boldsymbol{X}$$

This corresponds to the Bloch Sphere in figure 3.13, with the given precession axes. The detuning can be pulsed rapidly, changing precession axis and angular velocity, such that arbitrary rotations on the Bloch sphere can be realized. Experimental gate fidelities are still below 99%, but there seems to be no theoretical reason why they could not be pushed up to that level.

3.3.4 *Relaxation*

Good discussions of relaxation can be found in [11] and [30]. The qubit subspace of the S-T_0 qubit is not the ground state. Below, there is the $|T_+\rangle$ state. Spin states only couple to magnetic fields, but spin orbit coupling mixes the spin and orbital states and the orbital states couple to the charge environment. This includes background charge fluctuations in the doping layer, fluctuations in the gate potentials and phonons. GaAs is piezoelectric, which leads to piezoelectric phonons that couple relatively to the charge environment. The RF-gates that control the detuning are connected to coaxial cables, that run all the way up to an arbitrary waveform generator outside the dilution refrigerator. The expected noise spectrum should be an attenuated room temperature spectrum. The photon and phonon density of states increases with the energy difference, thus relaxation processes increase with the energy difference between the occupied and the ground state.

During the readout, usually taking a certain amount of time, the singlet is the ground state. If there is a relaxation event during the measurement time, a triplet events is identified as a singlet. This can be corrected if the relaxation rate is known, but it depends on the magnetic field and the readout point. One can correct for this effect by taking a histogram of the readout of successively prepared triplet states, the singlet component

3.3.5 *Two Qubit Gates*

Originally, the Loss-DiVincenzo proposal suggested two qubit gates via the exchange interaction, but this would require precise dynamic control of the tunnel coupling between different DQDs. This has not been shown experimentally, yet. The controlled coupling of two double quantum dot qubits has been demonstrated by coulomb interaction [31]. This type of gate could work for any singlet-triplet qubit,

but the gate takes place in a configuration that couples strongly to charge noise, which might limit the achievable fidelity.

3.3.6 *Summary*

There are initialization and readout schemes that work for any singlet triplet qubit. Coulomb interaction based two qubit gates would also work for either singlet triplet encoding. For the S-T_0 qubit, universal single qubit control has been achieved and single qubit gate fidelities could be pushed to the limit required for a working quantum computer. [32]

4

LANDAU-ZENER PHYSICS AT THE S-T_+ TRANSITION

What is usually called Landau-Zener physics derives from a series of papers in 1932 [33, 34, 35, 36, 37] and should really be named Landau-Zener-Stückelberg-Majorana physics, because all of these researchers have contributed to the understanding of the problem.The Landau-Zener model is one of the most widely used models in the physics of driven two-level systems along with the Rabi model. The reason for the wide use of the Landau-Zener model is, that it has an analytic solution and often applies approximately.

Recent focus on the Landau-Zener model comes from the fact, that it is a special case of the strongly driven two-level system. This has been of interest in the quantum information community, especially in superconducting qubits [38] and double quantum dot charge qubits [39]. Here I will focus on double quantum dot spin qubits.

4.1 THE LANDAU-ZENER FORMULA

A good review of Landau-Zener physics can be found in [40]. Of the 1932 papers, Majorana's paper is closest to the subject of this thesis. It is about the transition probability of a spin-$1/2$ subject to a fixed finite field in x-direction and a time dependent field in z-direction. Today we write the Hamiltonian as

$$\widehat{H} = \frac{\varepsilon(t)}{2}\boldsymbol{Z} + \Delta\boldsymbol{Y},$$

$\varepsilon(t)$ is called detuning and Δ is the transition matrix element or coupling. In the Landau-Zener scenario, the detuning is a linear function of time $\varepsilon(t) = \alpha t$. This is a good assumption in case of a narrow crossing, because in the crossing region, the variation will be approximately linear. The coupling Δ is never turned off, but it becomes irrelevant as ε becomes big. Landau, Zener and Majorana all found the solution if the detuning is swept from $-\infty$ to ∞.

There are different ways to solve this problem and they are found in the five original papers as is nicely explained in [41], which compares the different approaches. One usually writes down the time dependent Schrödinger equation:

$$i\hbar\frac{\partial}{\partial t}\begin{pmatrix} C_0 \\ C_1 \end{pmatrix} = \begin{pmatrix} \frac{\alpha t}{2} & \Delta \\ \Delta & -\frac{\alpha t}{2} \end{pmatrix} \quad \begin{pmatrix} C_0 \\ C_1 \end{pmatrix}$$

This can be decoupled by taking a time derivative and substituting the formula itself to get a second order differential equation. Note that all parameters except the coefficients C_0 and C_1 are real.

$$\ddot{C}_0 + \left(\frac{\alpha^2 t^2}{4} + \Delta^2 - i\frac{\alpha}{2}\right) C_0 = 0$$
$$\frac{1}{\Delta}\left(i\dot{C}_0 - \frac{\alpha t}{2} C_0\right) = C_1$$

Now the second order differential equation can be integrated for t from via contour integration in the complex plane. A thoroughly explained solution for non-mathematicians can be found in [42]. It is also possible to just look up differential equations in a compendium of functions and find out, that this particular equation is solved by Weber functions, which is what Zener did. The good thing about this is, that one can also derive a finite time Landau-Zener propagator, which describes the time evolution after a linear sweep in energy. With this, one can derive the axis and angle of a Landau-Zener unitary, which can be found in [43].

In the context of this thesis, only the transition probability for an infinite sweep is interesting, which is well known as the Landau-Zener probability:

$$P_{LZ} = 1 - \exp\left(-\frac{2\pi\Delta^2}{\hbar\alpha}\right)$$

For more sophisticated approaches, the nuclear spin averaging explained in section 4.1.2 and the calculation of correlations of successive sweeps in section 4.2 would not be so straightforward.

4.1.1 *The* $S - T_+$ *Transition*

The S-T_+ Transition is a narrow avoided crossing mediated by the perpendicular Overhauser field difference between the dots and spin orbit interaction. The detuning ε can be controlled with RF pulses from an arbitrary waveform generator, sweeps speeds can range from slow adiabatic transitions to the near-sudden limit.

Around the S-T_+ transition, one can derive an effective Hamiltonian on the relevant subspace containing $|T_+\rangle$ and

$$|S^*(\varepsilon)\rangle = \cos\psi |S(1,1)\rangle + \sin\psi |S(0,2)\rangle,$$

the lower energy singlet eigenstate. The angle ψ is called mixing angle and depends on the tunnel coupling between the dots. Other states are energetically separated. In the $[|S^*\rangle, |T_+\rangle]$ basis, the Hamiltonian is of the Landau-Zener-Stückelberg-Majorana Hamiltonian form:

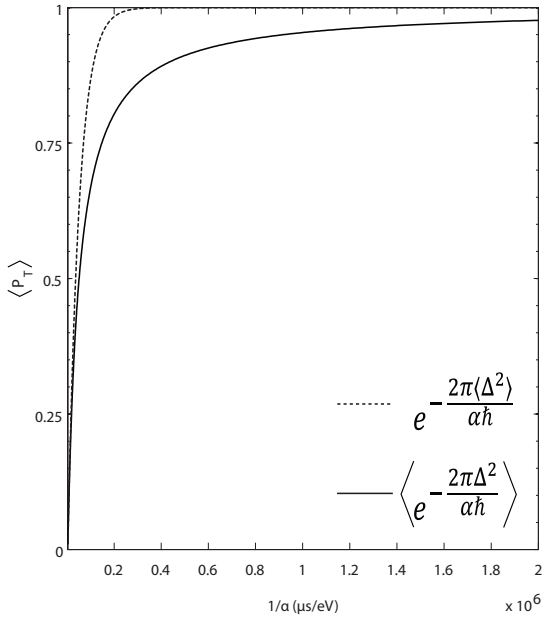

Figure 4.2: Triplet probability as a function of inverse sweep speed mean nuclear field and the nuclear spin averaged triplet probability.

$$\mathbf{H} = \frac{B_{\text{ext}} + \overline{B}^{z}_{\text{nuc}} - J(\varepsilon)}{2}\boldsymbol{Z} + \Delta \boldsymbol{X} \tag{4.1}$$

The $\overline{B}^{z}_{nuc}$ shifts the crossing's position, this can be in the same order of magnitude as the width of the crossing. A control with rectangular pulses, similar to the S-T_0 qubit would therefore be difficult, because frequency and axis of oscillations depend strongly on the position of the crossing and the matrix element coupling it. $\overline{B}^{z}_{nuc}$ can be controlled within limits, but the S-T_+ oscillations would slightly change it. Landau-Zener like pulses sweeping a large energy range close to the crossing would not be sensitive to slight changes in the position of the crossing. More importantly, as will be shown in section 4.1.2, the matrix element Δ is subject to uncontrollable dynamics.

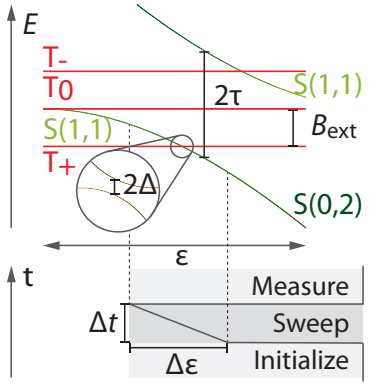

Figure 4.1: Energy diagram and Landau-Zener Sweep for the S-T+ Transition

4.1.2 *Nuclear Spin Averaged Landau-Zener Probability*

For our specific crossing, the Landau-Zener probability changes due to noise in the off-diagonal matrix element Δ. This matrix element is given by transverse effective magnetic fields from spin-orbit coupling and nuclear spins:

$$\Delta = \left| \mathbf{\Omega}^{\perp} \sin\psi + \delta \boldsymbol{B}^{\perp}_{\text{nuc}} \cos\psi \right| . \tag{4.2}$$

While $\mathbf{\Omega}^{\perp}$ is assumed to be fixed, $\delta \boldsymbol{B}^{\perp}_{\text{nuc}}$ is a statistical variable; the nuclear spins are highly disordered. $\delta \boldsymbol{B}^{\perp}_{\text{nuc}}$ is also subject to dynamics on a μs scale. These dynamics do not need to be taken into account during the sweep, because the relevant time spent at the crossing is in the ns range. This means that $\delta \boldsymbol{B}^{\perp}_{\text{nuc}}$ will be a different constant for each individual sweep.

The other contribution to Δ from SO coupling $\mathbf{\Omega}^{\perp}$, depends on the tunnel rate between the dots, the inter-dot distance and the position of the dot-dot axis with respect to the crystal axes. Therefore the effective field from SO coupling is expected to be static. The expected effective field from SO coupling is on the order of 100 mT, but it is suppressed by the mixing angle that favors $|S(1,1)\rangle$ at low external magnetic fields.

The expectation value of the measured triplet probability can be calculated by nuclear spin averaging. As explained in section 3.2.2, the nuclear spin effective field is normally distributed in each component for each species, denoted by index i. $\delta B^x_i = 1/2 \left(\delta B^x_{R,i} - \delta B^x_{L,i} \right)$, with a standard deviation σ_i that contains fluctuations of the field in each dot. The σ_i are calculated as suggested in section 3.2.2.

In the following, I am going to neglect the mixing angle. One can think of it as incorporated into the $\mathbf{\Omega}^{\perp}$ and $\delta \boldsymbol{B}^{\perp}_{\text{nuc}}$, but for experiments It is assumed without loss of generality, that the spin-orbit field points in the $x$direction.

$$\begin{aligned}
\langle P_T \rangle &= \left\langle 1 - \exp\left(-\frac{2\pi\Delta^2}{\hbar\alpha} \right) \right\rangle \\
&= 1 - \prod_i \int \dots \int d\delta B^x_i d\delta B^y_i \frac{1}{2\pi\sigma_i^2} \exp\left(-\frac{\left(\delta B^x_i\right)^2 + \left(\delta B^y_i\right)^2}{\sigma_i^2} \right) \\
&\quad \cdot \exp\left(-\frac{2\pi}{\hbar\alpha} \left(\left(\delta B^x_i + \Omega\right)^2 + \left(\delta B^y_i\right)^2 \right) \right) \\
&= 1 - \frac{\hbar\alpha}{\hbar\alpha + 4\pi \sum_i \sigma_i^2} \cdot \exp\left(-\frac{2\pi\Omega^2}{\hbar\alpha + 4\pi \sum_i \sigma_i^2} \right)
\end{aligned}$$

Thus, the nuclear spin averaging leads to a change from exponential to algebraic behavior in the transition probability as a function of sweep speed. If the spin orbit contribution was dominant, the exponential behavior should be recovered, because it is not subject to similar averaging. That means that one can learn about the amount of spin orbit coupling by the shape of the curve of the triplet probability as a function of sweep speed, that is shown in figure 4.2.

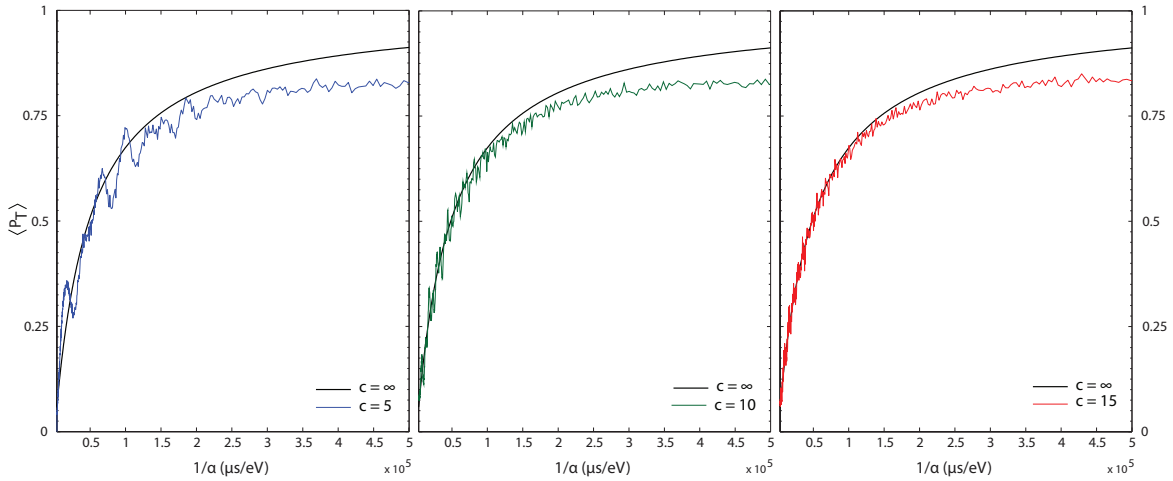

Figure 4.3: Finite sweep effects. Solid curve is the nuclear spin averaged triplet probability from chapter 4.1.2. Colored curves correspond to symmetric sweeps across the transition from $-c\langle\Delta^2\rangle$ to $c\langle\Delta^2\rangle$ in energy. For c=5 one can see oscillations around the infinite sweep solution, but for c=15 those oscillations are barely visible against the noise.

4.1.3 *Finite Sweep Effects*

The Landau-Zener Formula is valid for sweeps from $-\infty$ to ∞. Theoretically a study of finite time effects and other effects, such as what happens if the sweep does not extend across the transition can be found in [44]. The finite coupling duration leads to oscillations in the transition probability, that have to do with the trivial phase collected over the sweep time.

In order to verify these results and check the effects of noise, I did a time discretization Monte Carlo simulation for the Landau-Zener problem. This is possible for a finite Landau-Zener problem and allows the introduction of noise in the next steps. The idea is to slice the time axis into small bits to calculate the unitary time evolution operator of the Landau-Zener sweep.

$$\begin{aligned} U_{LZ} &= \mathcal{T} \exp\left(-\frac{i}{\hbar}\int_{t'=t_i}^{t'=t_f} \widehat{H}\left(t'\right) dt'\right) \\ &= \prod_{t_i}^{t_f} \exp\left(-\frac{i}{\hbar} H\left(t_i\right) dt\right) \end{aligned}$$

In case of a two-level system this only requires the multiplication of 2x2 matrices, the matrix exponential can be easily written out for the Pauli Matrices. The time steps need to be small compared to the energy splitting at any point, in this case Δ is the crucial parameter.

Assuming a negligible spin-orbit contribution, $\langle\Delta^2\rangle = \langle\left(\delta B^{\perp}\right)^2\rangle = {}^1/_2\sum_i \sigma_i^2 \approx 90\,\text{neV}$, this corresponds to a timescale of $\approx$45 ns. For the simulations I picked a step size of 0.1 ns.

To investigate finite sweep effects, I simulated symmetric Landau-Zener sweeps for different sweep speeds. As a measure for sweep range I used the size of the crossing itself with a constant c: $-c\langle\Delta^2\rangle$ to $c\langle\Delta^2\rangle$. Curves for three different ranges can be found in figure 4.3. For short range sweeps there are additional oscillations around the infinite sweep curve. But the oscillations are already weak for $c = 10$ and disappear in the noise at $c = 15$. One can reach a sweep ranges where the infinite sweep approximation is valid and the Landau-Zener formula holds. However, it is important, that the sweep does not extend to low detuning, because there the T_0 level would have to be considered.

I also investigated the effect of the non-linear transfer function. Experimental sweeps were linear in ε rather than in $J(\varepsilon)$, because this is practically easier to realize but in the case of a narrow avoided crossing this should not introduce a large error. To check this, I have simulated linear sweeps in $J(\varepsilon)$ and ε with identical speeds at the crossing to compare the results. For larger c this does not introduce a significant deviation, the only effect is that for small c the oscillations in the triplet probability change as seen in figure 4.4. They are regular for the linear sweep in energy, the exponential transfer function leads to more complicated behavior. In principle it should be possible to calculate a finite time Landau-Zener probability for exponential sweeps, but this would involve complicated contour integration.

4.1.4 *Diagonal Noise - Electrical Noise*

In experiment one has to take into account that the solid state environment is noisy. Not only the nuclear spins contribute to that, but electrostatic noise. Noise that is slow on the scale of a Landau-Zener sweep and not strong enough to shift the transition out of the sweep range would not have a great effect on the triplet probability.

But noise that is fast compared to the sweep speed could lead to multiple transitions. Fast white noise leads to a completely mixed state, as shown analytically in [45]. There are claims that a high frequency noise environment could lead to a dressed reduced coupling [46]. Landau-Zener Processes could be used to probe high frequency noise in a system in the same way, that spin-echo sequences are used to probe low frequency noise.

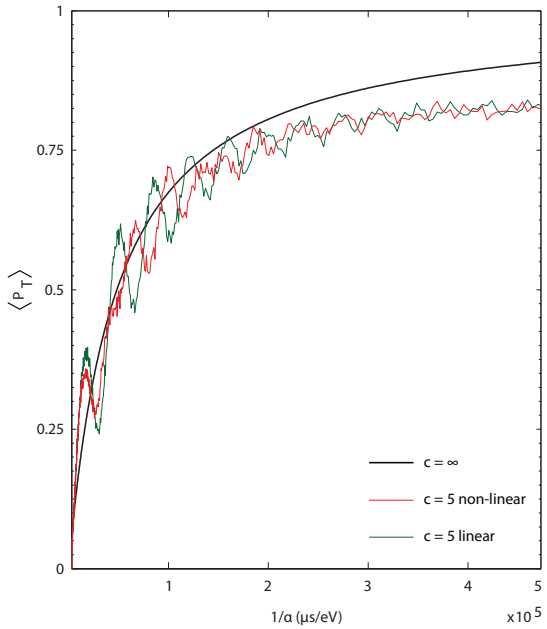

Figure 4.4: Effect of the non-linearity. There is a change in the oscillations, they are more regular for the linear case.

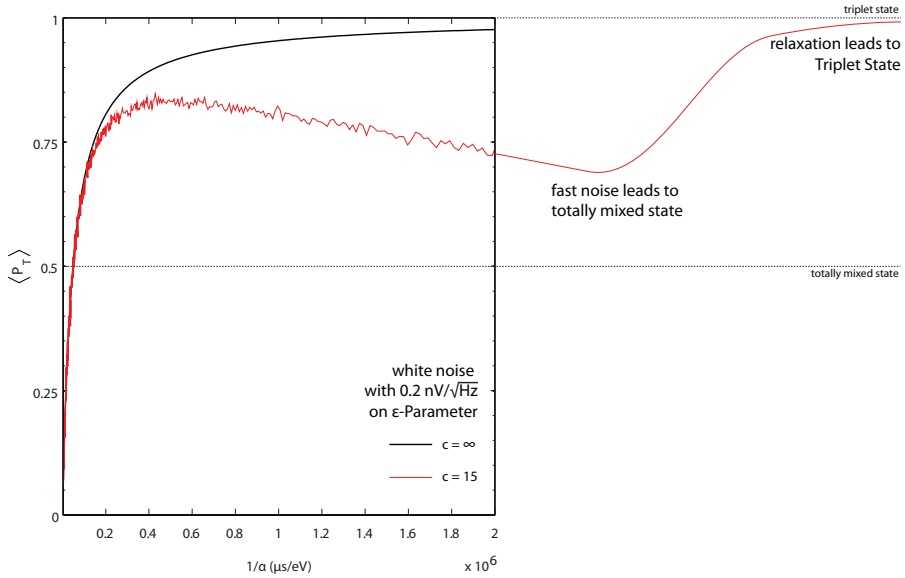

Figure 4.5: Triplet probability for slower sweep speeds. In accordance with [45] there is a reduction in triplet probability. For even slower sweeps relaxation should lead to $\langle P_T \rangle = 1$, experimentally one should be able to observe the competition between the two mechanisms.

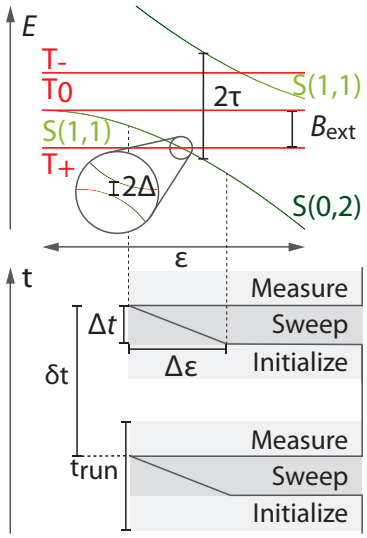

Figure 4.6: Energy diagram and Landau-Zener Sweep for the S-T+ Transition

4.2 CORRELATION OF LANDAU-ZENER SWEEPS

The nuclear spin dynamics are negligible on the timescale of single sweeps, but they can be probed by taking correlation measurements as suggested in [47]. One can take successive Landau-Zener sweeps with a fixed time in between and measure the triplet outcome, as shown in figure 4.6. The run time is mainly limited by the measurement time which is ob the order of 1 μs. Initialization is pretty fast, the sweep time depends on the sweep range and sweep speed but will probably not exceed a few μs.

From the measurement outcomes and the known timescales in between, the average auto-correlations is computed as a function of the time delay. It takes the form $\langle P_T(t)\, P_T(t+\delta t)\rangle$. The time resolution is only limited by the accuracy of pulse timing, but not by the required averaging time. Only the first data point is limited by the time t_{run} that single run takes.

$$\begin{aligned}\langle P_T(t)\, P_T(t+\delta t)\rangle &= \left\langle \left(1-\exp\left(-\frac{2\pi}{\hbar\alpha}\Delta(t)^2\right)\right)\right. \\ &\qquad \left.\cdot\left(1-\exp\left(-\frac{2\pi}{\hbar\alpha}\Delta(t+\delta t)^2\right)\right)\right\rangle \\ &= 1-2\left\langle \exp\left(-\frac{2\pi\Delta^2}{\hbar\alpha}\right)\right\rangle \\ &\qquad +\left\langle \exp\left(-\frac{2\pi}{\hbar\alpha}\left(\Delta(t)^2+\Delta(t+\delta t)^2\right)\right)\right\rangle \end{aligned} \tag{4.3}$$

The second term was calculated above, the third term contains the dynamics in the matrix element due to precession in the external magnetic field. Writing down the time dependence of the coupling parameter can be done compactly by introducing $\boldsymbol{\delta B}_i^{\pm} = \boldsymbol{\delta B}_i^x \pm i\boldsymbol{\delta B}_i^y$. The time dependence can be written in terms of exponential functions, $\boldsymbol{\delta B}_i^{\pm}(t+\delta t) = \boldsymbol{\delta B}_i^{\pm}(t)\exp(\pm i\omega_i \delta t)$

$$\begin{aligned}\Delta^2(t+\delta t) &= \left|\boldsymbol{\Omega}^{\perp} + \boldsymbol{\delta B}_{\text{nuc}}^{\perp}(t+\delta t)\right|^2 \\ &= \Omega^2 + \sum_{i,j} \boldsymbol{\delta B}_i^{+}(t)\ \boldsymbol{\delta B}_j^{-}(t)\ \exp\left(i\left(\omega_i - \omega_j\right)\delta t\right) \\ &\quad + \sum_i \Omega\left(\boldsymbol{\delta B}_i^{+}(t)\exp(i\omega_i\delta t) + \boldsymbol{\delta B}_i^{-}(t)\exp(-i\omega_i\delta t)\right)\end{aligned}$$

For $\Omega = 0$, one can see there are oscillations with the difference frequencies, as expected, because the nuclear spins precess in the external field without a fixed frame of reference. For $\Omega > 0$, there are rotations with the actual frequencies ω_i. The calculation of the third term in equation 4.3 is a technical issue. There is a way of avoiding solving the general integral described in section 4.2.1, but I have solved the integral for three spin species and no spin orbit coupling:

$$\left\langle \exp\left(-\frac{2\pi}{\hbar\alpha}\left(\Delta(t)^2 + \Delta(t+\delta t)^2\right)\right)\right\rangle$$

$$= \frac{(\hbar\alpha)^2}{(\hbar\alpha)^2 + 8\pi\hbar\alpha\sum_i \sigma_i^2 - 32\pi^2\sum_{i,j}\sigma_i^2\sigma_j^2\left(\cos\left(\left(\omega_i - \omega_j\right)t\right) - 1\right)}$$

A solution like this is useful for benchmarking. The integral is also solvable for spin-orbit coupling, but the formula is lengthy and I have not found a way to generalize it to additional spin species used to model nuclear spin dephasing as explained in section 3.2.2.

4.2.1 *T-matrix method*

The $\left\langle \exp\left(-\frac{2\pi}{\hbar\alpha}\left(\Delta(t)^2 + \Delta(t+\delta t)^2\right)\right)\right\rangle$ term can be evaluated without solving the general integration. The basic idea is to rewrite the exponent in terms of a dimensionless complex variable $\delta B_\alpha^{\pm} = \sigma_\alpha z_\alpha^{\pm}$ as done in [13]. The $z_\alpha$will be normally distributed with an rms of 1. Taking the factor $\frac{2\pi}{\hbar\alpha}$ into the matrix and vector elements, the exponent can be rewritten as

$$\sum_{i,j} \boldsymbol{T}_{ij} z_i^{+} z_j^{-} + \sum_i \left(\boldsymbol{V}_i z_i^{+} + \boldsymbol{V}_i^{*} z_i^{-}\right) + \Omega^2,$$

with

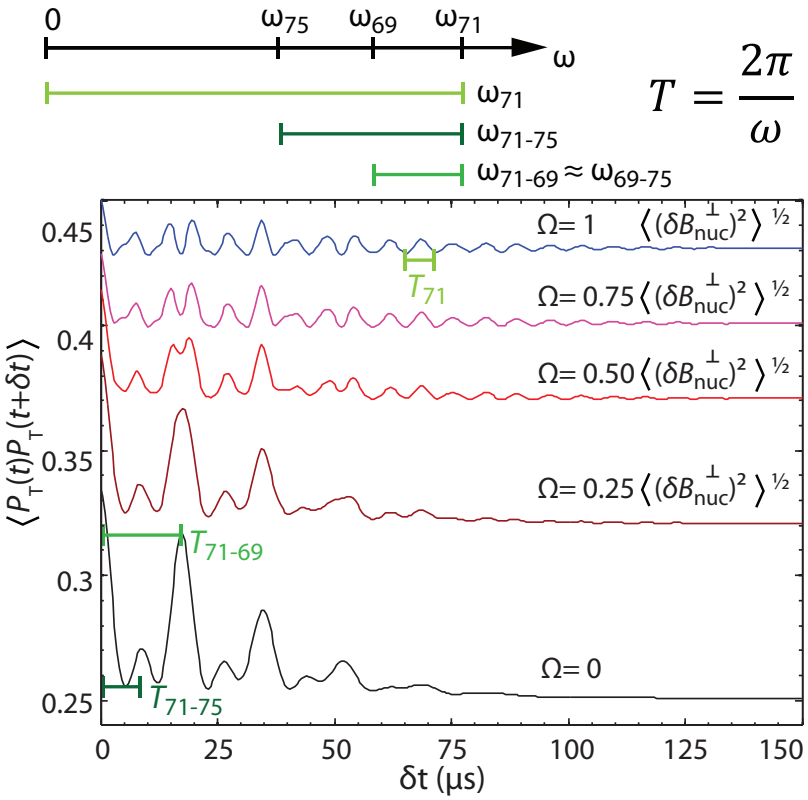

Figure 4.7: Simulations of correlations for different SO coupling, different periods for nuclear spin species are given. $\delta B_{\mathrm{loc}} = 0.3\,\mathrm{mT}$ and $N = 2 \cdot 10^6$. For $\Omega = 0$, correlations oscillate with relative frequencies. For $\Omega > 0$ additional raw frequencies appear, most importantly the peaks are split, but there are also fast, long lasting oscillations and a broadening of the peaks.

$$\boldsymbol{T}_{ij} = \frac{2\pi}{\hbar\alpha}\left(1 + \exp\left(i\left(\omega_i - \omega_j\right)t\right)\right)\sigma_i\sigma_j$$
$$\boldsymbol{V}_i = \frac{2\pi}{\hbar\alpha}\Omega\left(1 + \exp\left(i\omega_i t\right)\right)\sigma_i.$$

The integration is complicated by the coupling of the normal-distributed random variables z_α. This can be resolved by diagonalizing the $\boldsymbol{T}$ matrix. For any numerical value of t, this can be done exactly. The remaining integral is relatively easy for each separate species:

$$\int\int dxdy \frac{1}{2\pi}\exp\left(-\frac{x^2+y^2}{2}\right)\cdot\exp\left(-\lambda\left(x^2+y^2\right) - vx\right)$$

$$= \frac{1}{1+2\lambda}\exp\left(\frac{v^2}{2\left(1+2\lambda\right)}\right)$$

λ is the eigenvalue of the $\boldsymbol{T}$-matrix for the respective species and v the element of the transformed into the eigenvector basis.

With this method I have simulated the correlations for different values of spin orbit coupling. Results are summarized in figure 4.7. Sweep speeds were adjusted such that $\langle \mathrm{P_T} \rangle \approx 1/2$, because this maximizes the contrast in the correlations data.

For $\Omega = 0$, one can see peaks that correspond to the relative alignment of nuclei with the relative frequencies. The large frequency gives smaller peaks, because it corresponds to two of the nuclear spin species aligning. At the smaller frequency all three nuclear spins species align. The reason is the peculiar distribution of the nuclear spin species: They are nearly equidistant. This means that the $\Omega = 0$ behavior is governed by two frequencies. Peaks are broadened by nuclear spin dephasing and the slight mismatch between ω_{71-69} and ω_{69-75}. Nuclear spin dephasing leads to a loss of correlations at about 80 ¯s, therefore the beating will only be visible at external magnetic fields of about 200 mT, assuming that the SO contribution does not dominate at that point.

Spin orbit interaction adds a steady background. With increasing Ω the overall correlations tend toward $\langle P_\mathrm{T}(t)\, P_\mathrm{T}(t+\delta t)\rangle \to \langle P_\mathrm{T}\rangle^2$. In the intermediate regime the raw nuclear frequencies appear as fast long lasting oscillations in the correlations. The most striking sign of spin orbit interaction is the splitting of the first large peak in the correlations.

These findings indicate that the method can provide direct, qualitative and quantitative evidence for SO coupling.

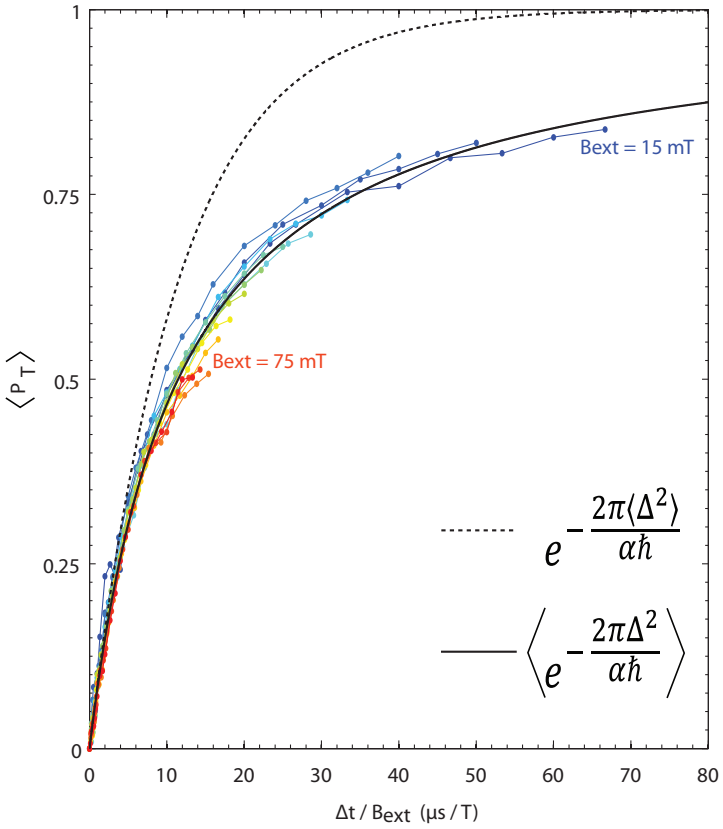

Figure 4.8: Triplet probabilities as a function of sweep-time Δt from 0 μs to 1 μs with a constant $\Delta\varepsilon$ for different $\boldsymbol{B_{ext}}$ in steps of 5 mT. Time axis rescaled with magnetic field shows reasonable collapse of the curves. Data in color. Dashed black line shows LZ-model of a mean nuclear field, solid black line shows the nuclear spin averaged Landau-Zener behavior. $N = 2 \cdot 10^6$ is set, α then requires a scaling factor of 7 to match experiment.

4.3 EXPERIMENTAL RESULTS

My adviser Hendrik Bluhm measured single sweeps and correlations in 2009 in Harvard with Sandra Foletti in the group of Amir Yacoby on samples produced by Diana Mahalu, Vladimir Umansky. The samples were similar to the one displayed in 3, but instead of a sensing dot he used a quantum point contact to read out the charge state of the dot. The background QPC voltage that is subject to noise was subtracted to get a better signal. Also the crossing's position was monitored. Only for one of the sweep times did the crossing move to a value in ε that was close to the sweep boundary, which is probably responsible for the bump seen in figure 4.8 for the blue curve close to $\Delta t = 0$ at $\langle P_T \rangle \approx 0.25$. For the other curves, the crossing was positioned well within the sweep range.

The results for single sweeps are given in figure 4.8. The exponential model of the transfer function means that the actual speed at the crossing can be approximated by:

$$\alpha = \left.\frac{\partial J}{\partial t}\right|_{\varepsilon_c} = B_{ext} \frac{1}{\varepsilon_0} \frac{\Delta\varepsilon}{\Delta t}$$

Knowledge of the transfer function is crucial to check our understanding of the system, because the Landau-Zener probability depends on sweep speed and matrix element. It is important to know both. One can check the model of the transfer function by rescaling the time axis, dividing by the external magnetic field. The curves should collapse on each other. In figure 4.8 one can see reasonable albeit not perfect collapse. The higher magnetic field curves seem to lie slightly above the spin averaged triplet probability, whereas the low magnetic curves seem to lie below. Relaxation during readout should be stronger for higher magnetic fields, reducing triplet visibility. In future experiments this effect could be monitored and corrected for by looking at the histograms of single shot outcomes, but the old data does not contain the necessary information to correct for this effect. There is also no sign of a decrease in triplet probability with increasing sweep time and the sweeps are not long enough to undoubtely identify the plateau.

A scaling factor of about 7 in α has to be introduced. The number of nuclei is fixed to $2 \cdot 10^6$ unit cells covered by the wave function. This could either mean, that the factor in the transfer function is wrong or we overestimate the matrix element. There might also be more relaxation than expected. To find out what causes this, additional experiments have to be done. The transfer function can be mapped out and rechecked. If this effect was due to noise, it should scale with the slope of the transfer function at the crossing and therefore the matrix element would shrink with increasing magnetic field. One can in

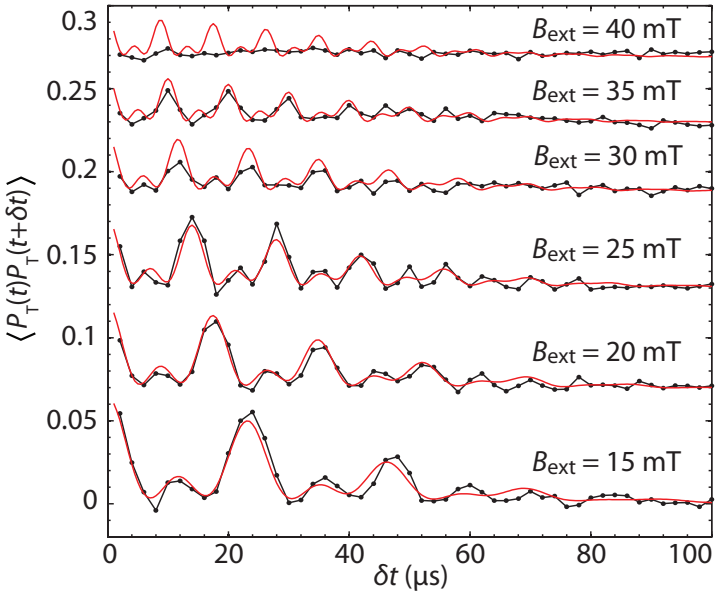

Figure 4.9: Correlation of triplet probabilities for different $\boldsymbol{B_{ext}}$, data in black and model in red. $N = 2 \cdot 10^6$, $\delta B = 0.3\,\mathrm{mT}$ are chosen, α requires a scaling factor of 20 to match experiment. Timescales of correlations are as expected and scale reasonably with $\boldsymbol{B_{ext}}$.

principle rule out relaxation by initializing triplet states and mapping out the relaxation as a function of detuning. Since these experiments, single shot readout has been improved, there s a good chance that theory and experiment can be brought together.

Results for the Landau-Zener correlations at different magnetic fields can be found in figure 4.9. Experimentally, the Landau-Zener cycles were just concatenated back to back. The correlation data points are 2 ¯s apart. The fit is most sensitive in α, which determines the contrast. The transition speed was not adjusted for different B_{ext} so that contrast varies because of fluctuations in $\langle \mathrm{P_T} \rangle$. For higher fields there are no distinguishable features any more. A different scaling factor has to be introduced to fit model to experiment . This only affects the contrast, not timescales of the oscillations and the decay, which are as expected for a local field rms value to $\delta B = 0.3\,\mathrm{mT}$. Therefore we conclude that our semi-classical model for the nuclear spins is supported by the experimental evidence. In future measurements, the sweep speed should be adjusted so that $\langle \mathrm{P_T} \rangle = 1/2$ to have maximum visibility in the oscillations. But there is no sign of spin orbit coupling. Introducing it into the fits does not give values that significantly deviate from 0. Also there are no indicators of additional frequencies. This is not surprising, because the data is taken at very low external fields,

where the mixing angle should suppress the spin orbit interaction at the crossing.

4.4 INVESTIGATING THE SPIN ORBIT INTERACTION

Deliberately looking for spin orbit effects and a better understanding of the S-T_+ transition could help to improve DNP methods and lead to improved qubit control. In the future more systematic experiments could distinguish the spin orbit and nuclear spin effects similar to [48]. A vector magnet would be helpful, to prove that one actually sees spin orbit effects, because the dependence on the crystal axis would help to establish that. Also, a top gate defined dot would help to identify spin orbit effects, because this would allow tuning the Rashba contribution.

The experiments would consist of gathering Landau-Zener sweep correlations for large external magnetic fields and with changing magnetic field direction in the 2DEG plane. To get accurate measurements of the matrix element, it is important to solve the problem of the scaling factors in section 4.3. Only with the knowledge of the sweep speed can Δ^2 be extracted from the triplet probabilities. If one could extract the mixing angle, this would make it possible to quantitatively identify the spin orbit and hyperfine contribution to the transition element. At higher magnetic fields the read out is sometimes compromised, which might limit the achievable magnetic field range one could probe. The direction dependence would make it possible to distinguish Rashba and Dresselhaus components.

One could look for weak spin orbit in the broadening of the first large correlation peak - beak width could be measured well, because the resolution is only limited by pulse timing which gives an upper limit in the ns range.

4.5 STÜCKELBERG INTERFEROMETRY

The pioneering work on Landau-Zener physics at the S-T+ Transition was actually not only on single sweeps, but focuses on Stückelberg interferometry [49]. Stückelberg interferometry refers to experiments where the crossing is traversed several times. The simplest case is a double crossing as displayed in figure 4.13. In the Landau-Zener limit, the crossing acts like a beam-splitter with a non-trivial phase ϕ, the corresponding time evolution operator is

$$U_{LZ} = \begin{pmatrix} \sqrt{1-P_{LZ}}e^{-i\phi} & -\sqrt{P_{LZ}} \\ \sqrt{P_{LZ}} & \sqrt{1-P_{LZ}}e^{i\phi} \end{pmatrix}.$$

Figure 4.10: Stückelberg Interferometry with more complicated Pulses

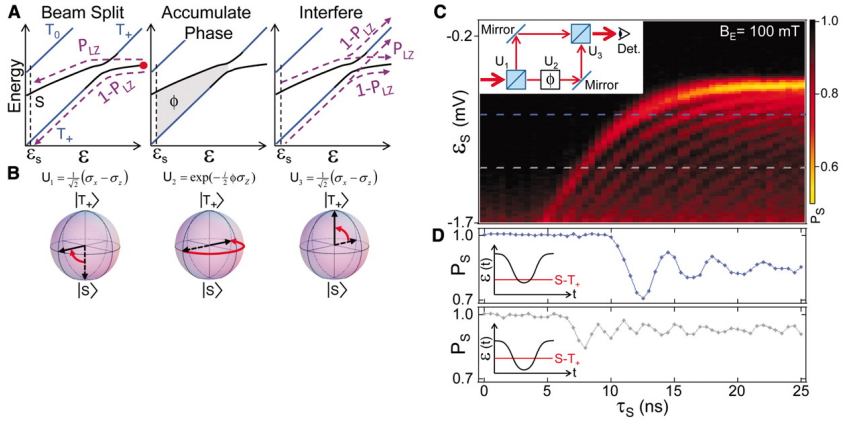

Figure 4.11: Stückelberg Interferometry Results from the first Petta publication [49]

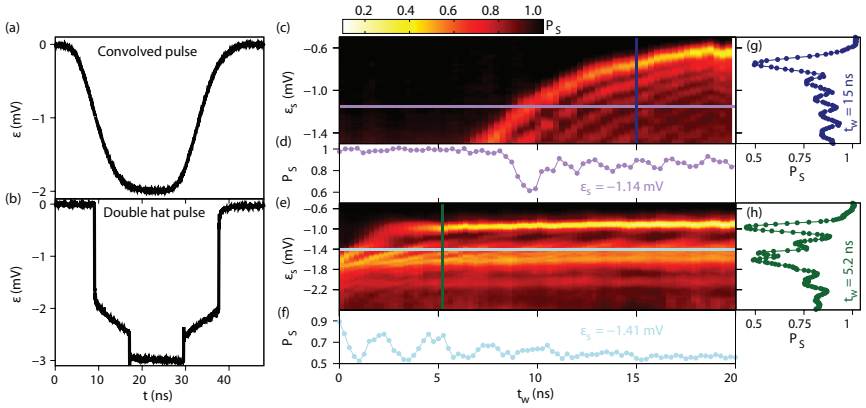

Figure 4.12: Stückelberg Interferometry with more complicated pulses leads to increased visibility of the oscillations Ribeiro et al. [50]

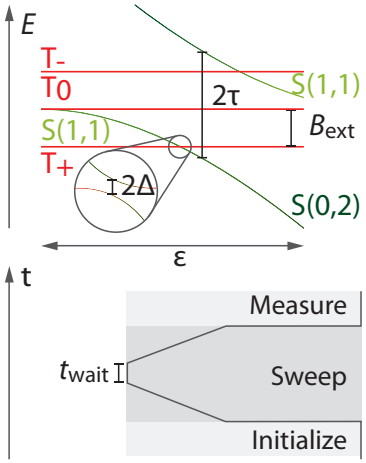

Figure 4.13: Scheme for Stückelberg interferometry

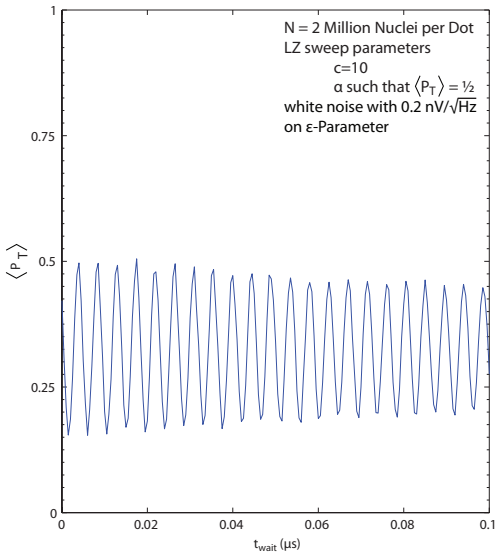

Figure 4.14: Simulation of the triplet probability

After the crossing, the system will be in a superposition of $|S\rangle$ and $|T_+\rangle$. Between the two crossings, a waiting time at constant detuning can be added. The phase of the superposition oscillates with the energy difference between $|S\rangle$ and $|T_+\rangle$. A second crossing will add an additional rotation, so that the triplet probability (Petta et al. report the singlet probability - fortunately one can be easily converted into the other) in the end depends on the waiting time. This corresponds to a Mach-Zehnder interferometer as suggested by the title of [49]. The observed observations in the triplet probability show the expected behavior: Changing the magnetic field changes the transfer function at the waiting point and thus the oscillation amplitude.

The Overhauser field has an influence on non-trivial phase in the beam-splitter Hamiltonian, but there should be no relevant fluctuations on the timescale of a sweep. Therefore nuclear spin noise should only reduce the visibility of the oscillations. However, noise in ε should contribute to the dephasing during the waiting time. Which of these contributions dominates should be testable by shifting the waiting point and seeing whether dephasing scales with the slope of the transfer function at that point. One could look for weak spin

I have simulated the Stückelberg interferometry to check whether the nuclear spin averaging in this thesis explains the visibility reported by Petta et al. I neglected nuclear dynamics, although in case of Stückelberg interferometry the change in the nuclear field direction might become relevant. Simulations show a visibility of about 30% in Stückelberg oscillations which about the maximum reported by Petta et al. The decay in figure 4.14 is unrealistically slow, because

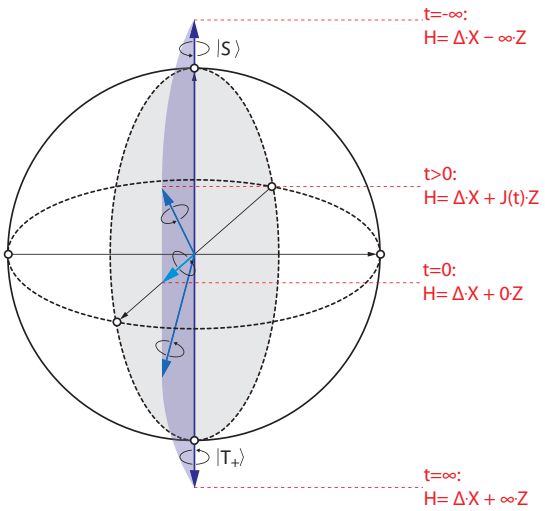

Figure 4.15: S-T_0 qubit Bloch Sphere with precession axes

I only took into account the fast charge noise contribution. The slow noise component might be corrected with spin-echo like pulses, but this has not been investigated in more detail.

In a follow up paper, Ribiero et al. reported, that the visibility of the oscillations can be increased with more elaborate pulses Ribeiro et al. [50], increasing the visibility to 50%.

4.6 REMARKS ON THE S-T_+ QUBIT

An S-T_+ Qubit relies on the same initialization and readout techniques as an S-To qubit, but until now the S-T_0 qubit outperforms its Landau-Zener counterpart. Using $|S\rangle$ and $|T_+\rangle$ state as computational subspace has been suggested by Ribiero and Burkard in [51] and in Ribiero's thesis [52]. The Bloch sphere with precession axes during a sweep is sketched in figure 4.15, but the $t = 0$ rotation axis generally has an x- and y-component, depending on Overhauser field direction. The z-axis is controlled via the detuning and should be fairly reliable.

The correlation at $\delta t = 0$ gives the variation in the triplet probability for a simple Landau-Zener pulse. For two million nuclear spins coupled to each electron, and a Landau-Zener sweep velocity tuned such that $\langle P_T \rangle = \frac{1}{2}$, the fluctuations would be on the order of $\left\langle (P_T)^2 \right\rangle \approx \frac{1}{3}$, thus an equal superposition of S and T_+ could only be produced with a standard deviation of $\sqrt{\frac{1}{3} - \frac{1}{4}} \approx 0.29$.

Accordingly, the randomness in the coupling parameter is a huge problem for controlling the "easy" $|S\rangle$-$|T_+\rangle$ axis on the Bloch sphere. It is not possible to tune this parameter with current dynamic nuclear polarization schemes, only for very high polarizations one could significantly reduce it. This would however require even faster pulses.

The speed in the publications by Petta et al. is already close to the current hardware limit.

This could be remedied by going to a spin-orbit dominated regime. There are different ways to reach this regime: In a certain range, one can increase the tunnel coupling. Also one can go to higher external magnetic fields and chose the direction of the magnetic field to maximize spin orbit coupling. But this also comes with drawbacks.

Control of the phase depends on the transfer function and is subject to fast electric noise on the detuning. Pulses take on the order of 10 ns, as demonstrated by Petta and others, which is an advantage, but in the same order of magnitude as pulse of the S-To qubit. In the spin orbit dominated regime, the transfer function is steeper around the transition, which means that the system is more sensitive to electrical noise.

A main advantage of the S-T_+ qubit is, that it has a longer relaxation time, but this depends on the regime in which it is operated. Relaxation is currently not limiting the performance of the S-T_0 or S-T_+ qubit, thus this is currently not relevant.

5

CONCLUSION AND OUTLOOK

In the level diagram of the two electron double quantum dot, the Landau-Zener transition is a narrow avoided crossing suitable for Landau-Zener physics. This refers to a linear sweep in the energy difference between the levels across the transition. The Landau-Zener formula is an analytic solution for the transition probability for a sweep from $-\infty$ to ∞ as a function of the matrix element coupling the levels and the sweep speed. In this case the matrix element is a sum of nuclear spin and spin orbit contributions.

The theoretical work in this thesis indicates that nuclear spin averaging and dynamics have to be taken into account for Landau-Zener physics at the S-T_+ transition. The Landau-Zener formula changes from an exponential to an algebraic behavior due to the averaging. Nuclear spin dynamics show up in the time dependend correlation of measurement outcomes for successive sweeps. Spin-orbit coupling also contributes to the Landau-Zener matrix element but is not subject to similar averaging and dynamics. This means that the Landau-Zener physics can be used to distinguish the spin orbit and hyperfine contribution.

The experiments of Landau-Zener are supporting the semi-classical nuclear spin model. The form of the triplet probability as a function of sweep speed is in qualitative agreement with the algebraic nuclear spin averaged Landau-Zener formula. A scaling factor has to be introduced to fit data and experiment. This needs to be investigated, but new measurements need to be taken, because these do not contain the information necessary to correct for relaxation which might account for the deviation.

The experimental correlations show the expected nuclear spin dynamics at the right frequencies and with a decay that is consistent with other experiments. The different scaling factor here is also not clear. In this low external field limit, it is expected that spin orbit coupling is suppressed by the mixing angle and as expected no spin orbit interaction effects are observed. But the observation of the correlations shows that those experiments are possible and already there is good qualitative agreement with theory. The nuclear spin dynamics and dephasing seen here are an important effect, because they are limiting DNP. The dynamics imply that the perpendicular component of the nuclei cannot be controlled unless one eliminates it by hyperpolarization, which is unlikely. It also means that the $\delta B_{\mathrm{nuc}}^{\perp}$ might go through so called dark states where $\delta B_{\mathrm{nuc}}^{\perp} \approx 0$ and be driven

back to $\delta B^{\perp}_{\mathrm{nuc}} > 0$ at a later time. Synchronizing DNP schemes with the dynamics would be good if $\delta B^{\perp}_{\mathrm{nuc}}$ was big to begin with, otherwise it would be detrimental, therefore desynchronizing and getting a good average might prove to be best. The nuclear dephasing is a mechanism that counteracts DNP, the local fields should be isotropic, therefore they also couple the $\delta B^{z}_{\mathrm{nuc}}$ to $\delta B^{\perp}_{\mathrm{nuc}}$.

In the future one could work out the exact impact of noise on the Landau-Zener problem to measure the high frequency noise component on ε. A precise knowledge of the noise spectral density could help to significantly improve gate fidelities of the DQD qubit [32]. Stückelberg interferometry could allow the measurement of the transfer function around the transition, but further away from the transition it might be limited by relaxation and the additional T_0 level.

The longtime goal of Landau-Zener experiments at the S-T_+ Transition would be to investigate the strength and direction of spin orbit coupling and use this knowledge to improve DNP schemes. It might also help to clarify the parameters of a DQD system, as spin orbit coupling is also an important factor in relaxation. An S-T_+ qubit does not show any significant advances over the more established S-T_0 qubit, except for longer relaxation times. But the matrix parameter would be more reliable if it was spin orbit dominated, so this regime needs to be investigated.

BIBLIOGRAPHY

[1] S. Haroche and J.-M. Raimond, Physics Today **49**, 51 (1996). (Cited on page 1.)

[2] M. Brune, E. Hagley, J. Dreyer, X. Maître, a. Maali, C. Wunderlich, J. Raimond, and S. Haroche, Physical review letters **77**, 4887 (1996), ISSN 1079-7114, URL http://www.ncbi.nlm.nih.gov/pubmed/10062660. (Cited on page 1.)

[3] C. Dawson and M. Nielsen, arXiv preprint quant-ph/0505030 (2005), 0505030v2, URL http://arxiv.org/abs/quant-ph/0505030. (Cited on page 5.)

[4] D. D. P. DiVincenzo, Fortschritte der Physik **48**, 771 (2000), ISSN 00158208, 0002077v3, URL http://arxiv.org/abs/quant-ph?0002077. (Cited on page 8.)

[5] D. Loss and D. P. DiVincenzo, Physical Review A **57**, 120 (1998), ISSN 1050-2947, URL http://link.aps.org/doi/10.1103/PhysRevA.57.120. (Cited on page 8.)

[6] D. P. DiVincenzo, D. Bacon, J. Kempe, G. Burkard, and K. B. Whaley, Nature **408**, 339 (2000), ISSN 0028-0836, URL http://www.ncbi.nlm.nih.gov/pubmed/11099036. (Cited on page 9.)

[7] J. Medford, J. Beil, J. M. Taylor, E. I. Rashba, H. Lu, a. C. Gossard, and C. M. Marcus, Physical Review Letters **111**, 050501 (2013), ISSN 0031-9007, URL http://link.aps.org/doi/10.1103/PhysRevLett.111.050501. (Cited on page 9.)

[8] W. a. Coish and D. Loss, Physical Review B **72**, 1 (2005), ISSN 1098-0121, URL http://link.aps.org/doi/10.1103/PhysRevB.72.125337. (Cited on page 13.)

[9] D. Stepanenko, M. Rudner, B. Halperin, and D. Loss, Physical Review B **85**, 075416 (2012), ISSN 1098-0121, URL http://link.aps.org/doi/10.1103/PhysRevB.85.075416. (Cited on pages 13 and 17.)

[10] K. C. Nowack, Ph.D. thesis, TU Delft (2009). (Cited on page 14.)

[11] R. Hanson, J. R. Petta, S. Tarucha, and L. M. K. Vandersypen, Reviews of Modern Physics **79**, 1217 (2007), ISSN 0034-6861, URL http://link.aps.org/doi/10.1103/RevModPhys.79.1217. (Cited on pages 14 and 22.)

[12] E. A. Chekhovich, M. N. Makhonin, A. I. Tartakovskii, A. Yacoby, H. Bluhm, K. C. Nowack, and L. M. K. Vandersypen, Nature materials **12**, 494 (2013), ISSN 1476-1122, URL http://www.nature.com/nmat/journal/v12/n6/abs/nmat3652.htmlhttp://www.ncbi.nlm.nih.gov/pubmed/23695746. (Cited on page 15.)

[13] I. Neder, M. S. Rudner, H. Bluhm, S. Foletti, B. I. Halperin, and A. Yacoby, Physical Review B **84**, 1 (2011), ISSN 1098-0121, URL http://link.aps.org/doi/10.1103/PhysRevB.84.035441. (Cited on pages 15 and 33.)

[14] H. Bluhm, S. Foletti, I. Neder, M. Rudner, D. Mahalu, V. Umansky, and A. Yacoby, Nature Physics **7**, 109 (2010), ISSN 1745-2473, URL http://www.nature.com/doifinder/10.1038/nphys1856. (Cited on pages 15 and 17.)

[15] D. Paget, G. Lampel, B. Sapoval, and V. Safarov, Physical Review B **15**, 5780 (1977), ISSN 0556-2805, URL http://onlinelibrary.wiley.com/doi/10.1002/cbdv.200490137/abstracthttp://prb.aps.org/abstract/PRB/v15/i12/p5780_1http://link.aps.org/doi/10.1103/PhysRevB.15.5780. (Cited on page 16.)

[16] H. Bluhm, S. Foletti, D. Mahalu, V. Umansky, and A. Yacoby, Physical Review Letters **105**, 216803 (2010), ISSN 0031-9007, URL http://link.aps.org/doi/10.1103/PhysRevLett.105.216803. (Cited on pages 17 and 21.)

[17] A. Higginbotham and F. Kuemmeth, arXiv pp. 1–5 (2013), 1306.2720v2, URL http://arxiv.org/abs/1306.2720. (Cited on page 17.)

[18] S. Mehl and D. DiVincenzo, arXiv (2013), 1305.0749v1, URL http://arxiv.org/abs/1305.0749. (Cited on page 17.)

[19] O. E. Dial, M. D. Shulman, S. P. Harvey, H. Bluhm, V. Umansky, and a. Yacoby, Physical Review Letters **110**, 146804 (2013), ISSN 0031-9007, URL http://link.aps.org/doi/10.1103/PhysRevLett.110.146804. (Cited on page 19.)

[20] C. Kloeffel, P. A. Dalgarno, B. Urbaszek, B. D. Gerardot, D. Brunner, P. M. Petroff, D. Loss, and R. J. Warburton, Physical Review Letters **106**, 046802 (2011), ISSN 0031-9007, URL http://link.aps.org/doi/10.1103/PhysRevLett.106.046802. (Cited on page 20.)

[21] C. Latta, A. Högele, Y. Zhao, a. N. Vamivakas, P. Maletinsky, M. Kroner, J. Dreiser, I. Carusotto, A. Badolato, D. Schuh, et al.,

Nature Physics **5**, 758 (2009), ISSN 1745-2473, URL http://www.nature.com/doifinder/10.1038/nphys1363. (Cited on page 20.)

[22] T. D. Ladd, D. Press, K. De Greve, P. L. McMahon, B. Friess, C. Schneider, M. Kamp, S. Höfling, A. Forchel, and Y. Yamamoto, Physical Review Letters **105**, 107401 (2010), ISSN 0031-9007, URL http://link.aps.org/doi/10.1103/PhysRevLett.105.107401. (Cited on page 20.)

[23] K. Ono and S. Tarucha, Physical Review Letters **92**, 256803 (2004), ISSN 0031-9007, URL http://link.aps.org/doi/10.1103/PhysRevLett.92.256803. (Cited on page 20.)

[24] J. Petta, J. Taylor, A. Johnson, A. Yacoby, M. Lukin, C. Marcus, M. Hanson, and A. Gossard, Physical Review Letters **100**, 067601 (2008), ISSN 0031-9007, arXiv:0709.0920v2, URL http://link.aps.org/doi/10.1103/PhysRevLett.100.067601http://prl.aps.org/abstract/PRL/v100/i6/e067601. (Cited on page 20.)

[25] I. T. Vink, K. C. Nowack, F. H. L. Koppens, J. Danon, Y. V. Nazarov, and L. M. K. Vandersypen, Nature Physics **5**, 764 (2009), ISSN 1745-2473, URL http://www.nature.com/doifinder/10.1038/nphys1366. (Cited on page 20.)

[26] S. Foletti, H. Bluhm, D. Mahalu, V. Umansky, and A. Yacoby, Nature Physics **5**, 903 (2009), ISSN 1745-2473, URL http://www.nature.com/doifinder/10.1038/nphys1424. (Cited on page 20.)

[27] M. Rudner, I. Neder, L. Levitov, and B. Halperin, Physical Review B **82**, 1 (2010), ISSN 1098-0121, URL http://link.aps.org/doi/10.1103/PhysRevB.82.041311. (Cited on page 21.)

[28] A. Brataas and E. I. Rashba, Physical Review B **84**, 045301 (2011), ISSN 1098-0121, URL http://link.aps.org/doi/10.1103/PhysRevB.84.045301http://prb.aps.org/abstract/PRB/v84/i4/e045301. (Cited on page 21.)

[29] A. Brataas and E. I. Rashba, arXiv (2012), 1206.0100, URL http://arxiv.org/abs/1206.0100. (Cited on page 21.)

[30] J. Taylor, J. Petta, A. Johnson, A. Yacoby, C. Marcus, and M. Lukin, Physical Review B **76**, 035315 (2007), ISSN 1098-0121, URL http://link.aps.org/doi/10.1103/PhysRevB.76.035315. (Cited on page 22.)

[31] M. D. Shulman, O. E. Dial, S. P. Harvey, H. Bluhm, V. Umansky, and A. Yacoby, Science (New York, N.Y.) **336**, 202 (2012), ISSN 1095-9203, URL http://www.ncbi.nlm.nih.gov/pubmed/22499942. (Cited on page 22.)

[32] P. Cerfontaine, Ph.D. thesis, RWTH Aachen (2013). (Cited on pages 23 and 46.)

[33] L. Landau, Physics of the Soviet Union 2 **1**, 88 (1932). (Cited on page 25.)

[34] Landau, Physics of the Soviet Union **1**, 46 (1932). (Cited on page 25.)

[35] C. Zener, Proceedings of the Royal Society A: Mathematical, Physical and Engineering Sciences **137**, 696 (1932), ISSN 1364-5021, URL http://rspa.royalsocietypublishing.org/cgi/doi/10.1098/rspa.1932.0165. (Cited on page 25.)

[36] E. Majorana, Il Nuovo Cimento (1924-1942) **9**, 43 (1932), URL http://www.springerlink.com/index/1108M7026W2M4448.pdf. (Cited on page 25.)

[37] E. Stueckelberg, Helvetica Physica Acta **5**, 370 (1932), URL http://scholar.google.com/scholar?hl=en&btnG=Search&q=intitle:Theorie+der+unelastischen+Stösse+zwischen+Atomen#0. (Cited on page 25.)

[38] W. D. Oliver, Y. Yu, J. C. Lee, K. K. Berggren, L. S. Levitov, and T. P. Orlando, Science (New York, N.Y.) **310**, 1653 (2005), ISSN 1095-9203, URL http://www.ncbi.nlm.nih.gov/pubmed/16282527. (Cited on page 25.)

[39] J. Stehlik, Y. Dovzhenko, J. R. Petta, J. R. Johansson, F. Nori, H. Lu, and A. C. Gossard, Physical Review B **86**, 3 (2012), ISSN 1098-0121, arXiv:1205.6173v2, URL http://prb.aps.org/abstract/PRB/v86/i12/e121303. (Cited on page 25.)

[40] S. Shevchenko, S. Ashhab, and F. Nori, Physics Reports **492**, 1 (2010), ISSN 03701573, URL http://linkinghub.elsevier.com/retrieve/pii/S0370157310000815. (Cited on page 25.)

[41] F. D. Giacomo and E. E. Nikitin, Physics-Uspekhi **48**, 515 (2005), ISSN 1063-7869, URL http://www.turpion.org/php/paper.phtml?journal_id=pu&paper_id=2804http://stacks.iop.org/1063-7869/48/i=5/a=A05?key=crossref.ccbe132765f17792ed2d291ac066ec1b. (Cited on page 25.)

[42] C. Wittig, The journal of physical chemistry. B **109**, 8428 (2005), ISSN 1520-6106, URL http://www.ncbi.nlm.nih.gov/pubmed/16851989. (Cited on page 26.)

[43] H. Ribeiro, J. R. Petta, and G. Burkard, Physical Review B **82**, 115445 (2010), ISSN 1098-0121, URL http://link.aps.org/doi/10.1103/PhysRevB.82.115445. (Cited on page 26.)

[44] N. Vitanov and B. Garraway, Physical review. A **54**, 5458 (1996), ISSN 1050-2947, URL http://www.ncbi.nlm.nih.gov/pubmed/9920648. (Cited on page 29.)

[45] Y. Kayanuma, Journal of the Physical Society of Japan **53**, 108 (1984), ISSN 0031-9015, URL http://jpsj.ipap.jp/link?JPSJ/53/108/. (Cited on pages 30 and 31.)

[46] R. S. Whitney, M. Clusel, and T. Ziman, Physical Review Letters **107**, 210402 (2011), ISSN 0031-9007, URL http://link.aps.org/doi/10.1103/PhysRevLett.107.210402. (Cited on page 30.)

[47] T. Fink and H. Bluhm, Physical Review Letters **110**, 010403 (2013), ISSN 0031-9007, URL http://link.aps.org/doi/10.1103/PhysRevLett.110.010403. (Cited on page 32.)

[48] M. Shafiei, K. C. Nowack, C. Reichl, W. Wegscheider, and L. M. K. Vandersypen, Physical Review Letters **110**, 107601 (2013), ISSN 0031-9007, URL http://link.aps.org/doi/10.1103/PhysRevLett.110.107601. (Cited on page 39.)

[49] J. R. Petta, H. Lu, and a. C. Gossard, Science (New York, N.Y.) **327**, 669 (2010), ISSN 1095-9203, URL http://www.ncbi.nlm.nih.gov/pubmed/20133567. (Cited on pages 39, 40, and 41.)

[50] H. Ribeiro, G. Burkard, J. R. J. Petta, H. Lu, and A. C. Gossard, Physical Review Letters **110**, 086804 (2013), ISSN 0031-9007, arXiv:1207.2972v1, URL http://link.aps.org/doi/10.1103/PhysRevLett.110.086804. (Cited on pages 40 and 42.)

[51] H. Ribeiro, J. Petta, and G. Burkard, arXiv (2012), 1210.1957v1, URL http://arxiv.org/abs/1210.1957. (Cited on page 42.)

[52] H. Ribiero, Ph.D. thesis, Universität Konstanz (2012), URL http://d-nb.info/1023210444/34. (Cited on page 42.)

COLOPHON

This document was typeset using the typographical look-and-feel `classicthesis` developed by André Miede. The style was inspired by Robert Bringhurst's seminal book on typography *"The Elements of Typographic Style"*. `classicthesis` is available for both LaTeX and LyX:

http://code.google.com/p/classicthesis/

Happy users of `classicthesis` usually send a real postcard to the author, a collection of postcards received so far is featured at:

http://postcards.miede.de/

Final Version as of October 1, 2013 (`classicthesis` version 4.1).

STATEMENT OF AUTHORSHIP

I hereby declare that this document has been composed by myself and describes my own work, unless otherwise acknowleged in the text. It has not been accepted in any previous application for a degree. All sources of information have been specifcally acknowledged in all conscience.

Aachen, September 2013

Christian Dickel